ISSN 2521-6368

Volume 8
Number 1
2024

Journal of Baku Engineering University

PHYSICS

Journal is published twice a year
Number - 1. June, Number - 2. December

An International Journal

http://journal.beu.edu.az

Contact address
Journal of Baku Engineering University
AZ0102, Khirdalan city, Hasan Aliyev str. 120, Absheron, Baku, Azerbaijan
Tel: *00 994 12 - 349 99 95* ***Fax:*** *00 994 12 349-99-90/91*

e-mail: *jr-phisics@beu.edu.az*
web: *http://journal.beu.edu.az*
facebook: *Journal Of Baku Engineering University*

ISSN 2521-6368

ISSN 2521-6368

Journal of Baku Engineering University

PHYSICS

Baku - AZERBAIJAN

Journal of Baku Engineering University

PHYSICS

2024. Volume 8, Number 1

CONTENTS

JOURNAL OF BAKU ENGINEERING UNIVERSITY - PHYSICS

2024. Volume 8, Number 1 ***Pages 3-8***

UOT: 621.315.592
PACS: 61.05.-a
PACS:65.40.-B
DOİ: https://doi.org/10.30546/09081.2024.101.5002

KINETICS OF STRUCTURAL PHASE TRANSFORMATIONS IN $K_{0.945}Ag_{0.055}NO_3$ and $K_{0.945}Cs_{0.055}NO_3$ MONOCRYSTALS

R.B.BAIRAMLI[1], V.I.NASIROV[2] , İ.M.MAHARRAMOV[3]
U.S. ABDURAHMANOVA[1], E. V. NASIROV[4]

[1]*Baku Engineering University*
[2]*Azerbaijan State Pedagogical University*
[3]*Military Scientific-Research İnstitute*
[4]*Azerbaijan Military Institute named after Heydar Aliyev, Baku*
Baku/AZERBAIJAN

ARTICLE INFO

Article history:
Received: 2024-06-03
Received in revised form: 2024-10-15
Accepted: 2024-10-17
Available online

Keywords: single crystal, polymorphic transformation, modification, kinetics, activation energy

ABSTRACT

In this work have been presented the result of investigation of $K_{0,945}Ag_{0,055}NO_3$ and $K_{0,945}Cs_{0,055}NO_3$ single crystals were grown from aqueous solution of KNO_3, $AgNO_3$ and $CsNO_3$ using isothermal crystallization method. Then, structural and phase transformations in samples were studied by X-ray and optical microscopy methods. It has been determined that in $K_{0,945}Ag_{0,055}NO_3$ monocrystal at T>393K temperature, in $K_{0,945}Cs_{0,055}NO_3$ monokrystal at T>455K temperature the rhombic (II) → hexagonal (III) transformation occurs with the formation and growth of the III - modification crystal embryo within II – modification. The results obtained from the kinetic studies were determined that the temperature dependence of the conversion rate of II → III in $K_{0,945}Ag_{0,055}NO_3$ and $K_{0,945}Cs_{0,055}NO_3$ single crystals can be expressed by an empirical formula of $\upsilon = (a\Delta T + b\Delta T^2 + c\Delta T^3) \cdot 10^{-2} \frac{cm}{sec}$. $\Delta T = T_t - T_0$ is temperature delay, $T_t -$ is transformation temperature and $T_0 -$ is equilibrium temperature between interconverting modification crystals. Based on the results of velocity measurements, the activation energy of II→III polymorphic transformations were calculated.

$K_{0,945}Ag_{0,055}NO_3$ və $K_{0,945}Cs_{0,055}NO_3$ MONOKRİSTALLARINDA QURULUŞ FAZA ÇEVRİLMƏLƏRİNİN KİNETİKASI

XÜLASƏ

İzotermik kristallaşma üsulu ilə KNO_3, $AgNO_3$ və $CsNO_3$-ün suda məhlulundan $K_{0,945}Ag_{0,055}NO_3$ və $K_{0,945}Cs_{0,055}NO_3$ monokristalları yetişdirilmiş, rentgenoqrafik və optik mikroskopiya üsulları ilə həmin nümunələrdə quruluş faza çevrilmələri tədqiq olunmuşdur. Müəyyən edilmişdir ki, $K_{0,945}Ag_{0,055}NO_3$ monokristalında T>393K temperaturda, $K_{0,945}Cs_{0,055}NO_3$ monokristalında isə T>455K temperaturda rombik (II) → heksaqonal (III) çevrilməsi II – modifikasiya daxilində III - modifikasiya kristalı rüşeyiminin yaranması və böyüməsi ilə gedir.

Kinetik tədqiqatlardan alınan nəticələr MATLAB proqramı əsasında işlənərək müəyyən edilmişdir ki, $K_{0,945}Ag_{0,055}NO_3$ və $K_{0,945}Cs_{0,055}NO_3$ monokristallarında II → III çevrilmə sürətinin temperatur asılılığı $\upsilon = (a\Delta T + b\Delta T^2 + c\Delta T^3) \cdot 10^{-2} \frac{sm}{san}$ emprik düsturu ilə ifadə oluna bilər. Burada $\Delta T = T_ç - T_0$ temperatur yubanması olub, $T_ç -$çevrilmə, $T_0 -$qarşılıqlı çevrilən modifikasiya kristalları arasında tarazlıq temperaturudur. Sürət ölçmələrinin nəticələri əsasında II → III polimorf çevrilmənin aktivləşmə enerjisi hesablanmışdır.

Açar sözlər: monokristal, polimorf çevrilmə, modifikasiya, kinetika, aktivləşmə enerjisi

КИНЕТИКА СТРУКТУРНЫХ ФАЗОВЫХ ПРЕВРАЩЕНИЙ В МОНОКРИСТАЛЛАХ $K_{0,945}Ag_{0,055}NO_3$ и $K_{0,945}Cs_{0,055}NO_3$

РЕЗЮМЕ

Монокристаллы $K_{0,945}Ag_{0,055}NO_3$ и $K_{0,945}Cs_{0,055}NO_3$ были выращены на водных растворах KNO_3, $AgNO_3$ и $CsNO_3$ методом изотермической кристаллизации. После этого структурные и фазовые превращения в этих образцах были изучены методами рентгеновской и оптической микроскопии. Установлено, что в монокристалле $K_{0,945}Ag_{0,055}NO_3$ при температурах T>393K, в монокристалле $K_{0,945}Cs_{0,055}NO_3$ при температурах T>455K происходит переход ромбическое (II) → гексагональное (III) превращение с образованием и ростом III – модификация кристаллического зародыша внутри II – модификации.

Результаты кинетических исследований были обработаны на основе программы MATLAB и установлено, что температурная зависимость скорости конверсии II → III в монокристаллах $K_{0,945}Ag_{0,055}NO_3$ и $K_{0,945}Cs_{0,055}NO_3$ может быть выражена эмпирической формулой $\upsilon = (a\Delta T + b\Delta T^2 + c\Delta T^3) \cdot 10^{-2}\,\frac{\text{см}}{\text{сек}}$. Здесь $\Delta T = T_{\text{п}} - T_0$ температурная задержка, $T_{\text{п}}$- температура превращения, а T_0 − температура равновесия между кристаллами взаимопревращающихся модификаций. По результатам измерений скорости рассчитана энергия активации полиморфных превращений II → III.

Ключевые слова: монокристалл, полиморфное превращение, модификация, кинетика, энергия активации.

Introduction

The investigation of structural transformations in potassium salts is of great scientific importance. Thus, the potassium salt crystals can be used as various converting devices, memory elements and heat radiation sensors. The structural transformation studies in the crystal and solid solutions of this substance can allow to determine its behavior in case of large dynamic loading (in the area of large deformation, explosions) or to eliminate the structural transformations during the application of this material. In addition, the results of the experiments can be applied in the methods of obtaining nanostructured materials.

The study of structural phase transformations in nitrate compounds of alkali metals, including potassium and silver nitrate crystals, is of great scientific and practical importance. Despite numerous experimental results, there is still no complete theory of the polymorphic transformation process. On the other hand, these substances are used for different purposes in different areas of our life. This includes the wide applications of these substances in explosives, glass production, drug preparation, robotics, solid rocket fuel preparation and other fields. In addition, these substances are used in the preparation of various converter devices, as memory elements and heat radiation transmitters [1, 2]. These investigations require studying the growth morphology of the modification crystals that are mutually transformed during these transformations. That is why the kinetics of structural transformations in $K_{0,945}Ag_{0,055}NO_3$ and $K_{0,945}Cs_{0,055}NO_3$ crystals have been studied in this work. The first two crystals are rhombic at room temperature and rhombohedral after structural transformation. *$CsNO_3$* has a trigonal lattice at room temperature, and a cubic lattice after transformation. All three of these transformations are enantiotropic and they are single crystal-single crystal type [3-9]. The crystallographic results of the polymorphic modifications of all three crystals and the temperature ranges of existence are represented in table 1.

Table 1. Crystallographic parameters of polymorphic modifications of KNO_3, $AgNO_3$ and $CsNO_3$ and temperature ranges of existence

Compound	Symmetry	Lattice parameters			Phase group	Existence temperature T,K	Reference
		a, Å	b, Å	c, Å			
KNO_3	Rhombic	5,411	9,164	6,431	*Pmcn*	300-400	3, 4
	Rhombohedral	5,43	-	9,112	$R\bar{3}m$	400-610	3, 4
	Rhombohedral	5,42	-	19,41	$R\bar{3}m$	397-383	5, 6
$AgNO_3$	Rhombic	6,997	7,325	10,118	Pbca	300-432,5	3, 7
	Rhombohedrik	5,203		8,522	$R\bar{3}m$	432,5-438	3, 7
$CsNO_3$	Trigonal	10,87	-	7,76	*P3/m*	300-434	3, 8
	Cubic	8,98	-	-	*Pa3*	434-687	9

In order to investigate the mechanism of structural transformations in the solid solutions of the compounds mentioned, a number of experiments were conducted and the results based on experiments was investigated [11-13].

Research method and research

Single crystals of $K_{0,945}Ag_{0,055}NO_3$ and $K_{0,945}Cs_{0,055}NO_3$ solid solutions were obtained by isothermal crystallization method from aqueous solutions of "ЧДА" type KNO3, AgNO3 and CsNO3 compounds, respectively. The samples were needle-shaped and planar plate-shaped. The length of the needle is oriented in the [001] crystallographic direction. The crystallization process was repeated several times in order to obtain perfect crystals. Among the obtained crystals, $1\times0.5\times10 mm^3$ crystals were selected for conducting microscopic studies.

Researches were carried out using a "Levenhuk C 310" type film camera in a MIN-8 brand polarizing microscope equipped with a special heater. The temperature of the crystal was measured using a copper-constantan thermocouple. The accuracy of the measurements was $\pm1^0C$ at 100^0C. Since the velocity measurements were carried out around the equilibrium temperature of the interconverting modification crystals, that temperature was determined first. It was determined that this temperature was 393 $\pm$1K for $K_{0,945}Ag_{0,055}NO_3$ and 455 $\pm$1K for $K_{0,945}Cs_{0,055}NO_3$.The temperature dependence of the new crystal growth rate during structure transformations was carried out by the method given in the work of [10].

During the experiments, the following were strictly observed:

1. The speed of movement of the boundary separating two modifications was measured only in the [001] crystallographic direction.
2. Only the rate of single-crystal-single-crystal conversion was measured.
3. During the experiment crystals of the same size and shape grown under the same conditions were used.

Measurements were made on six samples of each composition and the results obtained are given in table 2.

Table 2. Results from velocity measurements on $K_{0,945}Ag_{0,055}NO_3$ and $K_{0,945}Cs_{0,055}NO_3$ crystals

	$K_{0,945}Ag_{0,055}NO_3$			$K_{0,945}Cs_{0,055}NO_3$		
ΔT,K	T_o,K	$\overline{\upsilon}_t \cdot 10^{-2}$ cm/sec	$\overline{\upsilon}_h \cdot 10^{-2}$ cm/sec	T_o,K	$\overline{\upsilon}_t \cdot 10^{-2}$ cm/sec	$\overline{\upsilon}_h \cdot 10^{-2}$ cm/sec
1		0,056	0,472		0,215	0,340
2		2,514	1,883		3,912	2,157
3		4,342	4,273		5,918	5,429
4		6,523	7,681		9,650	10,138
5		12,635	12,150		14,513	16,263
6	**393±1**	18,240	17,717	**455±1**	23,420	23,783
7		24,438	24,425		32,226	32,679
8		32,525	32,314		44,745	42,432
9		40,521	41,423		55,322	54,519
10		52,241	51,793		66,356	67,423

In figures 1 and 2 the graps of results obtained by the experiments and the empirical formula are represented for the temperature dependence of the rate of structural transformations in $K_{0,945}Ag_{0,055}NO_3$ and $K_{0,945}Cs_{0,055}NO_3$ crystals, respectively. The experimental results are met with the theoretical calculations and it can be observed in graphs.

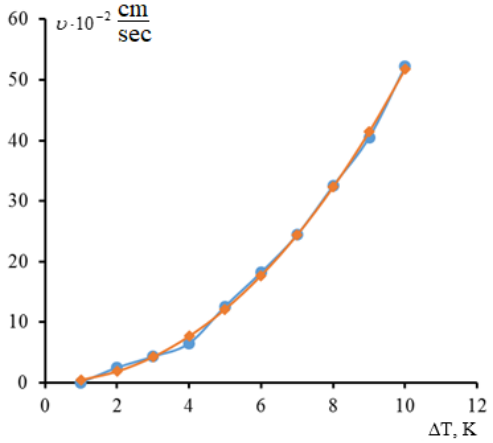

Figure 1. Graph of temperature dependence of growth rate of III-modification crystal in II→III transformation in $K_{0,945}Ag_{0,055}NO_3$ crystal. •-empirical datas; ◊-experimental datas

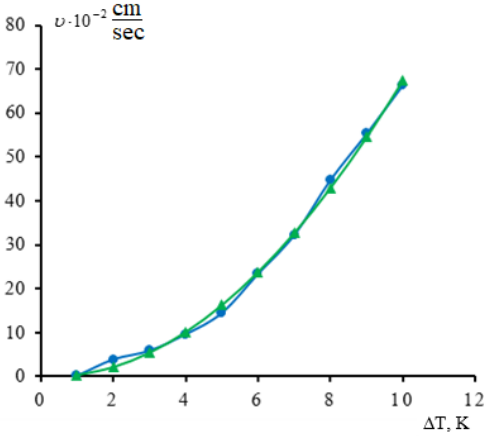

Figure 2. Graph of temperature dependence of growth rate of III-modification crystal in II→III transformation in $K_{0,945}Cs_{0,055}NO_3$ crystal. •-empirical datas; Δ- experimental datas

Conclusion

The conclusion of the obtained results showed that the mentioned partial replacement leads to an increase in the conversion speed. At a temperature of 10K this speed is is $52 \cdot 10^{-2}$cm/sec in $K_{0,945}Ag_{0,055}NO_3$, and $66 \cdot 10^{-2}$cm/sec in $K_{0,945}Cs_{0,055}NO_3$. /sec, while in KNO_3 is $5x10^{-2}$cm/sec as shown in table 2. In other words, as a result of this substitution, the rate of structure transformation has increased approximately 10 times. We think that partial replacement of K^+ ions by Ag^+ and Cs^+ ions in KNO_3 causes the energy barrier height to decrease. So, the speed is determined by the factor of $\upsilon \approx e^{\frac{E}{kT}}$, where E is the activation energy of the process. The activation energy is calculated based on the velosity mesurement results.

In order to evaluate the process of polymorphic transformation in terms of energy, the equation [14] given by M. Folmer for crystal growth from the liquid phase with a two-dimensional mechanism has been used:

$$\upsilon = \kappa_1 \, exp(-\frac{\kappa_2}{T_0}) \, exp(-\frac{\kappa_3}{T_0 \Delta T})$$

When this equation is applied to crystal growth during polymorphic transformation, k_2-is a constant that takes into account the energy limit necessary for the transfer of molecules from the parent crystal to the surface of the newly grown crystal and it is equal to $\frac{E}{R}$. Here E is the activation energy per 1 mole, R is the universal gas constant. In the equation T_0- is the equilibrium temperature between modifications, ΔT – is the temperature delay. k_1=Bνd and ν- is oscillation frequency of molecules, d- is interatomic distance, B- is number of molecules passing from parent crystal to growing crystal surface, k_3- is energy used for generation of two-dimensional crystal embryo. The Folmer equation also agrees well with the results obtained from velocity measurements on $K_{0,945}Ag_{0,055}NO_3$ and $K_{0,945}Cs_{0,055}NO_3$ crystals and the dependence slope of lnυ on $\frac{1}{T_0 \Delta T}$-is a straight line. According to the inclination of that straight line, k_2 and k_3 coefficients were determined, and the activation energy of II→III transformation was calculated in the studied crystals. The obtained results are given in table 3.

Table 3. Values of coefficients k_2, k_3 and activation energy in II→III transformation for $K_{0,945}Ag_{0,055}NO_3$ and $K_{0,945}Cs_{0,055}NO_3$ single crystals.

Content	k_2,deg^{-1}	k_3,deg^{-2}	Activation energy E, kJ/mol
$K_{0,945}Ag_{0,055}NO_3$	10877,5	4028,4	90,38
$K_{0,945}Cs_{0,055}NO_3$	12392,8	4121,9	102,98

As can be seen from Table 3, the rate of rhombic→hexagonal transformation in the $K_{0,945}Ag_{0,055}NO_3$ crystal increases as the temperature increases and the partial replacement of K+ ions by Ag+ ions in KNO_3 leads to a decrease in the activation energy. So, while the activation energy of the rhombic→hexagonal transformation for potassium nitrate is 97.8 kJ/mol, for $K_{0,945}Ag_{0,055}NO_3$ is 90.38 kJ/mol. On the other hand, the activation energy is 102.98 kJ/mol in the II→III transformation in the $K_{0,945}Cs_{0,055}NO_3$ crystal.

REFERENCES

1. J.F.Scott, Ferroelectric memories, Springer-Verlag Berlin Heidelberg, Germany, 2000.
2. Е.П. Теслева "Исследование полиморфных превращений в ионно-молекулярных диэлектриках методами физической акустики и теплофизики", Канд. Диссертация, Казан, 2006.

3. C.N.R. Rao, Crystal structure transformations in inorganic nitrites, nitrates, and carbonates / C.N.R. Rao, B. Prakash, M. Natarajan. – Washington: National Standard Reference Data System-National Bureau of Standards, p. 48. 1975.
4. J. K. Nimmo; and B. W. Lucas, A Neutron Diffraction Determination of the Crystal Structure of α-Phase Potassium Nitrate at 25^0C and 100^0C. J. Phys. C., 6, p. 201-211, 1973
5. J.K. Nimmo, and B. W. Lucas the Crystal Structures of γ- and β-KNO3 and the α-γ-β Phase Transformations. Acta Cryst. B., B-32, p. 1976.
6. Oswaldo Dieguez and Daid Vanderbilt, "Theoretical Study of Ferroelectric Potassium Nitrate" Phys. Rew B, Vol. 76, pp.134101, 2007.
7. P.U. Sastry, Krishna Psr., L. Panicker, A.B. Shinde Structural behavior of $AgNO_3$ at low temperatures by neutron diffraction. J. Phys. Indian Acad. Sci. Vol.71, p.929-933, 2008.
8. D. Pohl, and T. Gross Cesium Nitrate (II) at 296-K. Ast Cryst. C., 49, 316-318, 1993
9. B. Zhou, T. Giavani, H. Bildsoe, J. Skibsted and H. Jakobsen J. Structure Refinement of $CsNO_3$ (II) by Coupling of N-14 MAS NMR Experiments with WIEN2k DFT Calculations. Chem. Phys. Let., 402, 1-3, 2005
10. В.И. Насиров Полиморфизм в оптически прозрачных кристаллах, Баку, с.166, 1997.
11. V.I. Nasirov, R.B. Bairamov The kinetics of polymorphic transformation in $K_{1-x}Cs_xNO_3$ (x=0,015; 0,035; 0,045) single crystals. ANAS Reports, Vol.72, No.1, p.29-33, 2016.
12. V.I. Nasirov, R.B. Bairamov and E.V.Nasirov Morphology and Kinetics og Polymorphic Transformations in $K_{0.965}Rb_{0.035}NO_3$ Single Crystals//Crystallography Reports,v.60,N.7,p.1-5,2015.
13. V.I. Nasirov, R.B. Bairamov and E.V. Nasirov Polymorphic Transformations in the $K_{0.945}Ag_{0.055}NO_3$ Single Crystal. Crystallography Reports, , v.65, N.2, p.309-313,2020
14. M. Volmer Kinetik der phasenbildung steincopt. Dresden and Leipzing. vol.3, p.38-56, 1939.

JOURNAL OF BAKU ENGINEERING UNIVERSITY - PHYSICS

2024. Volume 8, Number 1 ***Pages 9-15***

UDC: 539.21
PACS: 68.65. Cd, 73.50. Bk
DOİ: https://doi.org/10.30546/09081.2024.101.5006

MAGNETIZATION OF DİLUTED MAGNETIC SEMICONDUCTOR II TYPE SUPERLATTICES WITH IMPURITIES Mn (manganese) IONS

Sophia R. FIGAROVA, Mehdi M. MAHMUDOV, Ragib Y. DAMIROV

Baku State University

Z. Khalilov Street, 23, AZ1148, Baku, Azerbaijan

ragibdamirov@bsu.edu.az, figarov@bsu.edu.az

ARTICLE INFO

Article history:
Received: 2024-10-08
Received in revised form: 2024-10-08
Accepted: 2024-10-15
Available online

Keywords:
diluted magnetic semiconductor,
II type superlattices,
quasi-two-dimensional electron gas,
magnetic impurity,
magnetization,
exchange interaction.

ABSTRACT

In this paper, the magnetization of diluted magnetic semiconductor superlattices with a magnetic impurity of manganese is studied. It was found that the magnetization of a quasi-two-dimensional electron gas, depending on the degree of filling of the miniband superlattices, the molar concentration of the impurity, the exchange interaction constant and the spin splitting factor, changes sign and in a strictly two-dimensional case becomes positive. In a magnetic field, magnetization oscillates, and in strong magnetic fields the oscillations weaken, and their amplitude and frequency decrease. The contribution of the impurity to the magnetization is calculated. In a relatively weak magnetic field the magnetization associated with the impurity increases linearly and at a certain condition to the depending on the magnitude of the exchange constant and the impurity concentration changes its sign.

НАМАГНИЧЕННОСТЬ ПОЛУМАГНИТНЫХ ПОЛУПРОВОДНИКОВЫХ СВЕРХРЕШЕТОК II ТИПА С ПРИМЕСЯМИ ИОНОВ Mn (марганца)

АННОТАЦИЯ

В данной работе исследуется намагниченность полумагнитных полупроводниковых сверхрешеток с магнитной примесью марганца. Найдено, что намагниченность квазидвумерного электронного газа в зависимости от степени заполнения минизоны сверхрешеток, молярной концентрации примеси, постоянной обменного взаимодействия и фактора спинового расщепления меняет знак и в строго двумерном случае становится положительной. В магнитном поле намагниченность осциллирует, причем в сильных магнитных полях осцилляции ослабевают, и их амплитуда и частота уменьшаются. Вычисляется вклад примеси в намагниченность. В относительно слабом магнитном поле намагниченность, связанная с примесью, возрастает линейно и при определенном условии в зависимости от величины обменной константы и концентрации примеси меняет знак.

Ключевые слова: полумагнитный полупроводник, сверхрешетки II рода, квазидвумерный электронный газ, магнитная примесь, намагниченность, обменное взаимодействие.

MANQAN İONLARI İLƏ AŞQARANMIŞ II NÖV YARIMMAQNİT YARIMKEÇİRİCİ İFRATQƏFƏSLƏRİN MAQNİTLƏNMƏ ƏMSALI

XÜLASƏ

İşdə manqan ionları ilə aşqaranmış yarımmaqnit yarımkeçirici ifratqəfəslərin maqnit xassələri tədqiq edilir. Tapılmışdır ki, minizonanın dolma dərəcəsindən, aşqarın molyar konsentrasiyasından, mübadilə qarşılıqlı təsir sabitindən və spin parçalanması faktorundan asılı olaraq kvaziikiölçülü elektron qazının maqnitlənmə əmsalı işarəsini dəyişir və ikiölçülü halda müsbət olur. Xarici maqnit sahəsində maqnitlənmə əmsalının ossilyasiya etdiyi təyin olunmuşdur. Belə ki, güclü sahələrdə bu ossilyasiyalar zəifləyərək onların amplitudu və tezliyi azalır. Maqnitlənmə

əmsalına maqnit aşqarının verdiyi pay da hesablanmışdır. Göstərilmişdir ki, zəif maqnit sahəsində aşqarla bağlı olan maqnitlənmə əmsalı xətti olaraq artır və müəyyən şərtdə mübadilə qarşılıqlı təsir sabitindən və aşqarın molyar konsentrasiyasından asılı olaraq işarəsini dəyişir.

Açar sözlər: yarımmaqnit yarımkeçirici, II növ ifratqəfəslər, kvaziikiölçülü elektron qazı, maqnit aşqarı, maqnitlənmə əmsalı, mübadilə qarşılıqlı təsir.

1. Introduction

Diluted magnetic semiconductor superlattices (DMSS), consisting of alternating layers of two materials that combine electronic and magnetic properties are perspective, and appear attractive both from the point of view of fundamental physics and technology. This is connected with to fact that superlattices exhibit many new electronic and optical properties, unusual for bulk samples, due to the presence of an additional periodic potential whose period is larger than the original lattice constant. In diluted magnetic semiconductor superlattices, it is possible to change the electronic potential after making the superlattice structure using external parameters such as the external magnetic field and temperature. Exchange interactions in such materials give rise to new spin-dependent phenomena, including giant spin band splitting and large Faraday rotation [2]. Due to the fact that in recent years it has become possible to quite accurately determine the values of exchange integrals, theoretical studies of the DMSS physical properties have received significant development. Changing the composition and impurities concentration in DMSS, lead to alteration the parameters of the band structure, i.e., magnetic impurities affect the properties of the semiconductor matrix; they also exhibit behavior characteristic of the paramagnetic and ferromagnetic phases with a change in the impurity concentration. The interaction between localized magnetic moments of an impurity and conduction electrons leads to a number of new properties, for example, the giant negative magnetoresistance at the semiconductor-semimetal transition [1]. All these effects have a common origin; they are caused by $sp-d$ exchange interactions. Many of theoretical and experimental works has been devoted to the study of the spin-dependent transport of charge carriers due to the reciprocity influence of transport and magnetic properties in DMS [2]. In recent years, using the MBE method, it has been possible to create layer systems with quantum wells and superlattices of good quality. However, there are significantly less studies in which low-dimensional systems are studied in the presence of a magnetic field and magnetic impurities [3-5]. As an example, we give heterostructures $GaAs/AlGaAs$ [6], where the impurity is manganese. The influence of the impurity localized magnetic moments is also manifested in the properties of two-dimensional electron gas in the DMS by changing the g factor. The magnitude of the g factor is affected by exchange interactions and temperature. Spin splitting reduces the g factor and changes the sign [7]. In this work, the DMSS thermodynamic properties, namely, magnetization, are studied, since statistical characteristics significantly affect the magnetic and transport properties of low-dimensional systems in the presence of a magnetic impurity. Impurity localized magnetic moments is also displayed in the properties of two-dimensional electron gas in the DMS by changing the g factor [8]. The magnitude of the g factor is affected by exchange interactions and temperature. Spin splitting reduces the g factor and changes the sign. In this work, the DMSS thermodynamic properties, namely, magnetization are studied, since statistical characteristics significantly affect the magnetic and transport properties of low-dimensional systems in the presence of a magnetic impurity.

2. Energy spectrum and density of states of DMSS

The possibility to create thin films, superlattices, and heterostructures of diluted magnetic semiconductors using molecular beam epitaxy in combination with the appearance of new properties of these materials makes low-dimension diluted magnetic semiconductors very important from the point of view of both basic research and applied sciences. In the $Cd_{1-x}Mn_xTe$ and $Hg_{1-x}Mn_xTe$ compounds, the exchange interaction between conduction electrons and $3d^5$ impurity electrons Mn is carried out in the mean-field approximation. For electrons in a given external magnetic field and for a given state of magnetic ions systems, in the case where the electron wave function is sufficiently delocalized and the influence of electrons on each of the magnetic ions can be neglected, the Hamiltonian has the form:

$$H = H_0 + H_B + H_C + H_{ex}, \tag{1}$$

where H_0 is the Hamiltonian of the electron in an ideal crystal; the term H_B describes the influence of the magnetic field on the electron's state this is responsible for Landau quantization and spin splitting; H_C describes the Coulomb interaction of carriers with impurities; and the term H_{ex} corresponds to the exchange interaction between carriers and ions.

Taking into account the electron spin $\mu_z B$ leads to an additional term in the Hamiltonian, where is $\mu_z = \mu_B(\sigma_z/\sigma)$ the projection of the intrinsic magnetic moment onto the field direction associated with the electron spin, σ_z - spin operator with eigenvalue $\pm 1/2$, $\mu_B = e\hbar/2m_0$ - Bohr magneton, *B* - magnetic field induction. Since the spin operator commutes with the Hamiltonian, its *z*th component is preserved, and in the Schrödinger equation, the spin and coordinate variables are separated. Therefore, the complete eigenfunctions of the electron, taking into account the spin, are obtained by multiplying the wave functions without spin by the spin wave functions corresponding to certain values of the spin projection $\sigma = \pm 1/2$ In this case, an additional term is added to the energy eigenvalues, corresponding to the energy of the eigenmoment in the magnetic field. The difference from a non-magnetic semiconductor is the presence of exchange interaction. For exchange interaction, the Heisenberg spin model:

$$H_{ex} = -\sum J(\vec{r} - \vec{R}_n) S_n \sigma, \tag{2}$$

n-number of the magnetic $J(\vec{r} - \vec{R}_n)$ ion, exchange integral between conduction band electrons and impurity electrons, σ - spin of mobile electrons with $\vec{r}$ radius vector, S_n - spin of magnetic impurity R_n localized at a site (for manganese $S_n = 5/2$). When the magnetic field is directed along z, then in H_{ex}, all manganese spin operators are replaced by their mean values, and for the conduction band, we have:

$$\langle \psi_c | H_{ex} | \psi_c \rangle = \begin{vmatrix} 3A & 0 \\ 0 & 3A \end{vmatrix}. \tag{3}$$

Here

$$A = -\frac{1}{6} N_0 \alpha \langle | S_z | \rangle x, \tag{4}$$

where N_0 is the number of cells per unit volume, the modification of the band structure caused by the *s-d* interaction will be described by a constant α equal to $\alpha = -\langle S|J|S\rangle/\Omega$, x - the

molar concentration of the impurity. In the Schrödinger equation, in the effective mass approximation, the exchange potential mixes the orbital and spin degrees of freedom, which can lead to the scattering of electrons from one orbital state to another with a spin flip. The solution to the Schrödinger equation with Hamiltonian (1) taking into account (3) for the energy spectrum of semimagnetic semiconductor superlattices in a strong magnetic field parallel to the axis directed perpendicular to z the layers, which quantizes the motion of the electron in the plane of the layer and removes the spin degeneracy for the energy spectrum, will have the form:

$$\varepsilon(N,\sigma,k_z) = (2N+1)\mu B + \varepsilon_0(1-\cos ak_z) + g^*\sigma\mu_B B + 3AS\,. \tag{5}$$

Where $N = 1,2,...$ are the Landau quantum numbers, k_z is the quasi-momentum component along the axis z, $\mu = (m_0/m_\perp)\mu_B$, m_0 is the mass of a free electron, $m_\perp$ is the mass of the electron in the plane of the layer, ε_0 is the half-width of the conduction band in the direction k_z, a is the superlattice period in the direction z, g^* is the factor that is determined from the band structure, and the rest are standard constants. It can be seen that each Landau level is distributed into two spin sublevels, and the magnitude of the distribution of the *N*th level is the same and equal to $\Delta\varepsilon = g^*\mu_B B$. In this work, manganese ions with spin 5/2 are taken as impurities, and then the energy spectrum (5) takes the form:

$$\varepsilon = (2N+1)\mu B \pm \frac{1}{2}g\mu_B B \mp \frac{5}{2}\alpha\, x\, f(B,T) + \varepsilon_0(1-\cos ak_z)\,. \tag{6}$$

x - molar concentration of manganese, $f(B,T) = \frac{2}{5}B_{5/2}\left(\frac{g_{Mn}\mu_B B}{k_0 T}\right)$, where

$$B_S(x) = \frac{2s+1}{2}cth\frac{2s+1}{2} - \frac{1}{2}cth\frac{x}{2}$$

- Brillouin function (at strong fields and low temperatures, this function tends to unity).

Two quasi-continuous determines one quantum state in a magnetic field (k_y, k_z), three discrete quantum numbers: N,σ,S and the density of states is determined by the formula:

$$g_B(\varepsilon) = \frac{1}{2(\pi R)^2 a}\sum_{N\sigma}(2\varepsilon_0\varepsilon_z - \varepsilon_z^2)^{-1/2} = \frac{1}{2(\pi R)^2 a\varepsilon_0}\sum_{N\sigma}\sin^{-1}(ak_z)\,, \tag{7}$$

Here $R = (\hbar/eB)^{1/2}$ - magnetic length, $\varepsilon_z = \varepsilon(N,\sigma,k_z) - (2N+1)\mu B - g^*\sigma\mu_B B - 3AS$,

$$Z(\varepsilon) = a\,k_z = \arccos\left(1 - \frac{\varepsilon-\varepsilon_z}{\varepsilon_0}\right).$$

From (7) it is clear that the density of states has a feature every time the energy coincides with one of the Landau levels $\varepsilon = \varepsilon_N = (2N+1)\mu B$, i.e. oscillates with changing magnetic field.

In the case of a degenerate electron gas, the density of states depends significantly on the relationship between the Fermi level and the width of the one-dimensional conduction band in the k_z direction. Taking spin splitting into account significantly affects the behavior of the density of state, and at large values of the g^* factor there is a linear dependence of the density of state on the magnetic field.

3. Magnetization

The magnetization of an electron gas M, using the Gibbs method, can be found based on the explicit form of the grand thermodynamic potential $\Omega = \Omega(T, V, \zeta, B)$:

$$M = -\frac{1}{V}\left(\frac{\partial \Omega}{\partial B}\right)_{T,V,\zeta}, \tag{8}$$

where the grand thermodynamic potential in a quantizing magnetic field has the form:

$$\Omega = -k_0 T \sum_{N k_y k_z S \sigma} \ln\left(1 + e^{\frac{\zeta - \varepsilon(N, k_z, S, \sigma)}{k_0 T}}\right). \tag{9}$$

For a grand thermodynamic potential $\Omega = \Omega(T, V, \zeta, B)$ we have:

$$\Omega = -k_0 T \frac{V}{2a(\pi R)^2} \sum_N \int_0^{z_0} \ln(1 + e^{\eta^* + \varepsilon_0^* \cos Z})\, dZ, \tag{10}$$

Where $\eta^* = \zeta^* - \varepsilon_N^* - \varepsilon_0^*$, $\zeta^* = \zeta / k_0 T$, $\varepsilon_N^* = \varepsilon_N / k_0 T$, $\varepsilon_0^* = \varepsilon_0 / k_0 T$ and the upper bound of the integral is defined as:

$$Z_0 = \begin{cases} \pi, & \varepsilon > 2\varepsilon_0 \\ \arccos\left(1 + \dfrac{\mu B + g\mu B/2 - 5\alpha x f(B,T)/2 - \varepsilon}{\varepsilon_0}\right), & \varepsilon < 2\varepsilon_0 \end{cases}. \tag{11}$$

If we move in (10) from integration over dZ to integration over $d\varepsilon$ energy, then for Ω we obtain [7]:

$$\Omega = \frac{k_0 T V}{2(\pi R)^2} \sum_{N S \sigma} \int_{\varepsilon_N}^{\infty} \frac{dk_z(\varepsilon, N)}{d\varepsilon} \ln\left(1 + \exp\left(\frac{\zeta - \varepsilon}{k_0 T}\right)\right) d\varepsilon. \tag{12}$$

The expressions are valid for any value of the magnetic field and the degree of degeneracy of the electron gas.

Taking into account (12) in (8), for magnetization, we obtain:

$$M = \frac{k_0 T}{B} \frac{1}{2a(\pi R)^2} \left\{ \sum_N \left[Z_0 + \frac{\mu_B B(2N+1)}{\varepsilon_0 \sin Z_0} \right] \ln\left[1 + \exp\left(\frac{\zeta - \varepsilon}{k_0 T}\right)\right] + \; + \frac{\varepsilon_0}{k_0 T} \int_0^{Z_0} f_0 Z \sin Z dZ \right\}. \tag{13}$$

In the case of a degenerate electron gas, for magnetization in the quantum limit $(N = 0)$ we have:

$$M = \frac{\varepsilon_0}{2a\pi^2 R^2 B} \left(\sin Z_0 - 2Z_0 \cos Z_0 - \frac{\mu B(1 + \sigma g^*) + 3AS}{\varepsilon_0} ctg\, Z_0 \right), \tag{14}$$

here Z_0 is given by formula (11).

From (14) it follows that the magnetization of a quasi-two-dimensional electron gas, depending on the degree of filling of the miniband, the molar concentration of the impurity, the exchange interaction constant and the g factor, changes sign and in a strictly two-dimensional case becomes positive. In a magnetic field, the magnetization oscillates, and in strong In magnetic fields, oscillations weaken, and their amplitude and frequency decrease. At low degrees of miniband filling, the magnetization has the form:

$$M = -\frac{\mu eB}{2a\pi^2 \hbar Z_0} + M_{Mn}. \tag{15}$$

The second term in equation (15) describes the contribution of the diluted magnetic semiconductor superlattces magnetization.

For magnetization, M_{Mn} we get:

$$M_{Mn} = \frac{5}{2} N \frac{(\mu_B g_{Mn})^2 B}{k_0 T} + \frac{\mu_B g_{eff}}{2} th\left(\frac{\mu_B g^* B}{k_0 T}\right), \tag{16}$$

where $g_{eff} = g^* - \frac{5}{2}\frac{\alpha x N}{\mu_B B}$.

In strong magnetic fields at low temperatures $\left(\frac{\mu g^* B}{k_0 T} >> 1\right)$, we have:

$$M_{Mn} = \frac{5}{2} N \frac{1}{k_0 T}\left(\mu_B g_{Mn}\right)^2 B + \frac{\mu_B g^*}{2}\left(1 - \frac{5}{2}\frac{\alpha x N}{\mu g B}\right). \tag{17}$$

Based on (17), it follows that with increasing magnetic field, the magnetization increases and then reaches saturation. At $\frac{\mu g^* B}{k_0 T} << 1$, i.e. at weak magnetic fields and high temperatures, the magnetization will be:

$$M_{Mn} = \frac{5}{2} N \frac{1}{k_0 T}(\mu_B g_{Mn})^2 B + \frac{(\mu_B g^*)^2 B}{4k_0 T}\left(1 - \frac{5}{2}\frac{\alpha x N}{\mu g B}\right). \tag{18}$$

From (18) it is clear that in a relatively weak magnetic field the magnetization increases linearly and at a certain magnetic field, but at $B < \frac{5}{2}\frac{\alpha x N}{\mu g^*}$, i.e. depending on the exchange constant and the concentration of the impurity, the sign changes.

4. Conclusion

The magnetization of DMSS with a magnetic impurity of manganese is being studied. It was found that the magnetization of a quasi-two-dimensional electron gas, depending on the degree of filling of the miniband, the molar concentration of the impurity, the exchange interaction constant and the g factor, changes sign and in a strictly two-dimensional case becomes positive. In a magnetic field, magnetization oscillates, and in strong magnetic fields the oscillations weaken, and their amplitude and frequency decrease. The contribution of the impurity to the magnetization is calculated. It is shown that this contribution in a strong magnetic field and at low temperatures increases with increasing magnetic field, and then reaches saturation as a result of the alignment of the spin of electrons and magnetic impurities in the averaged external magnetic field and the exchange field of the magnetic ion. In a relatively weak magnetic field, the magnetization associated with the impurity increases linearly and, at a certain magnetic field, depending on the exchange constant and the concentration of the impurity, changes sign.

REFERENCES

1. Furdyna J. K. Diluted magnetic semiconductors. J. Appl. Phys., 64(4), p. R29-R64, 1988.
2. Kacman P. Spin interactions in diluted magnetic semiconductors and magnetic semiconductor structures. Semiconductor Science and Technology. Vol. 16, Issue 4, p. R25-R39, 2001.
3. Gupta A., Zhang R., Kumar P., Kumar V., Kumar A. Nano-structured dilute magnetic semiconductors for efficient spintronics at room temperature. Magnetochemistry, Vol. 6(1), p. 15, 2020.
4. Babanli A.M., Ibragimov B.G. Magnetic moment of electrons in diluted magnetic semiconductor quantum ring. In Proc. of the 6th Inter. Conf. Cont. Opt. Ind. Appl. Vol. 1, p. 122-124, 2018.
5. Berry Habte Dulla. Thermodynamic properties of diluted magnetic semiconductors ($A_{1-x}Mn_xA'$ (A= Zn, Cd and A′= S, Te, Se)) using Heisenberg spin model in 3D. J. Appl. Phys. Sci. Inter. ol. 2(3), p. 101-106, 2015.
6. Ricardo de Sousa J., Branco N. S. Two-dimensional quantum spin-1 2 Heisenberg model with competing interactions. Phys. Rev. B, Vol. 72(13), p. 134421-1-4, 2005.
7. Bhatt R. N., Berciu M., Kennett M. P., Wan X. Diluted magnetic semiconductors in the low carrier density regime. Journal of Superconductivity: Incorporating Novel Magnetism, Vol. 15, No. 1, p. 71-83, 2002.
8. Zawadzki W. Theory of optical transitions in inversion layers of narrow-gap semiconductors. Journal of Physics C: Solid State Physics, Vol. 16(1), p. 229-240, 1983.

2024. Volume 8, Number 1 *Pages 16-25*

UOT: 531.1
***PACS:** 73.30. + y, 73.40.Ei*
DOİ: https://doi.org/10.30546/09081.2024.101.5008

STUDY OF DIELECTRIC PROPERTIES AND POWER DISSIPATION OF PTSI/N-SI SCHOTTKY DIODES AS A FUNCTION OF ALTERNATING SIGNAL

I.M. AFANDIYEVA, Ch.G.AKHUNDOV, N.A.RAHIMOVA

Baku State University

Baku, Azerbaijan

Corresponding author: I.M.AFANDIYEVA

afandiyeva@mail.ru, I_afandiyeva@yahoo.com

ARTICLE INFO

Article history:
Received: 2024-10-09
Received in revised form: 2024-10-18
Accepted: 2024-10-21
Available online

Keywords: Schottky diode, dielectric parameters, ac-conductivity, power dissipation, alternating voltage

ABSTRACT

The dielectric properties and power dissipation of PtSi/n-Si Schottky diodes of small area ($8x10^{-6}$ cm^2) were studied when the bias voltage varied in the range -2V ÷ 4V at room temperature. The amplitude of the alternating signal (V_{ac}) varied from 5 mV to $1x10^3$ mV. Studies based on impedance measurements revealed the dependence of dielectric parameters (ε', ε"), ac-conductivity (σ_{ac}) and power dissipation (P) only at V_{ac} = 200 mV. The obtained result is explained by the inhomogeneity of polarization and surface states.

1. Introduction

Most elements of modern solid-state electronics are based on contact structures with a Schottky barrier. The many advantages of these structures compared to n-junctions are of interest for the creation of multifunctional devices. Simple technology, a wide selection of materials, and the ability to manufacture densely packed structures are the basis for the fabrication of devices with low material costs and high performance capabilities. High speed due to charge transfer is carried out by the main charge carriers. Small dimensions of contact structure provide high packing density of elements on the crystal [1-3]. The miniaturization of semiconductor structures brings to the fore the task of rapidly improving the technology for obtaining and studying micro- and nanostructures and their rapid introduction into industrial production. The main goal of modern electronics is the development of multifunctional, stable, small-sized devices with low power dissipation.

The multifunctionality of the devices is achieved due to the sensitivity of the device and the ability to control it when operating factors change in a narrow range [4]. Taking into account the relevance of the topic, we investigated PtSi/n-Si Schottky diodes with small geometric dimensions and equipped with a diffusion barrier. Platinum silicide was used as the metal film of the diode. Interest in silicide is due to its high conductivity and temperature stability. Besides, PtSi is of interest for infrared applications due to its high work function [4,6].

Platinum silicide (PtSi) is formed due to chemical reaction between platinum (Pt) and silicon (Si). In such contact structure, the interface between silicide and silicon is formed in the semiconductor, which eliminates the influence of the environment and minimizes the density of surface electronic states [4-6].

An important role in the formation of barriers in contact structures is played by the crystal structure of the metal film and the crystallographic orientation of silicon [4-6]. The presence of silicides ensures the production of barriers with guaranteed adhesion of the metal to silicon and better mating of the lattices of the two materials. On the other hands reducing the size of devices puts forward the problem of the appearance of fluctuations in parameters. During the process of formation of a silicide compound on the surface of silicon, a rearrangement of atoms occurs continuously. As a result of the formation of the interfacial layer inhomogeneities are likely to appear, which can influence on the electrical and dielectric properties of this structure [7,8].

The purpose of studying the influence of an alternating signal on the properties of a PtSi/n-Si Schottky diode is connected by the several reasons. Firstly, the studied diodes have a small geometric area (~10^{-6} cm^2). Second, it is known that aluminum (Al) has a high diffusion coefficient. In order to prevent the penetration of Al through the silicide film, a diffusion barrier (an amorphous $Ti_{10}W_{90}$ alloy) was placed between PtSi and Al.

Third. Previous studies of diodes revealed the presence of self-assembled patches with a high impurity concentration [9]. The surface states of a PtSi/n-Si Schottky diode and their distribution were previously studied by us as functions of temperature and frequency, the dielectric characteristics were studied as functions of frequency [10-13]. We have studied the dielectric characteristics of diodes with the simultaneous application of dc- and ac- voltage. Dielectric losses, which characterize the conversion of a part of electrical energy into thermal energy, are an important electrophysical parameter of contact structures. The magnitude of these losses indicates the features of the polarization mechanism. Dielectric losses usually change to a large extent when various kinds of impurities are introduced into the dielectric and are a sensitive indicator of changes in the structure of the dielectric. The study of dielectric losses and their dependence on structural defects and various factors (temperature, dc- and ac-voltage, and frequency of test signal, etc.) is of considerable interest for modern electronics [14]. Our previous studies were devoted to studying the dependence of the dielectric parameters of PtSi/n-Si and Pd_2Si/n-Si diodes on frequency, temperature and illumination intensity based on admittance spectroscopy (20 mV peak to peak) [10-13].

The obtained results revealed that the highest values of dielectric losses ε'' and $tan\delta$ correspond to a frequency of 500 kHz and a temperature of 300 K. However, currently, the scientific literature does not pay attention to the study of the influence of amplitude of ac-voltage on dielectric parameters, resistance and conductivity and the power dissipation of PtSi/n-Si diodes.

2.Materials and methods

To fabrication the studied PtSi/n-Si diodes with small geometric dimensions ($8x10^{-6}sm^2$), the photolithography method was used. Characteristics of the semiconductor substrate are - monocrystalline silicon n-Si (111), a resistivity silicon wafer is 0.7 Ω·cm, diameter about 3 inches, thickness is 3.5 μm. A platinum film with a thickness of about 0.6 μm was obtained on a pre-cleaned surface of single-crystalline silicon wafer. Then the Pt/n-Si plate was annealed at a pressure of 6×10^{-5} Torr at 773 K and in an atmosphere of N_2 and H_2 gases [10-13,15].

The amorphous $Ti_{10}W_{90}$ diffusion barrier was deposited on the silicide film (PtSi) by magnetron sputtering method [15-17]. On a semiconductor matrix, was fabricated 14 diodes, areas of which changed from $1x10^{-6}$ cm^2 to $14x10^{-6}$ cm^2) (Fig.1). Geometric area of investigated diode is A=$8x10^{-6}$ cm^2.

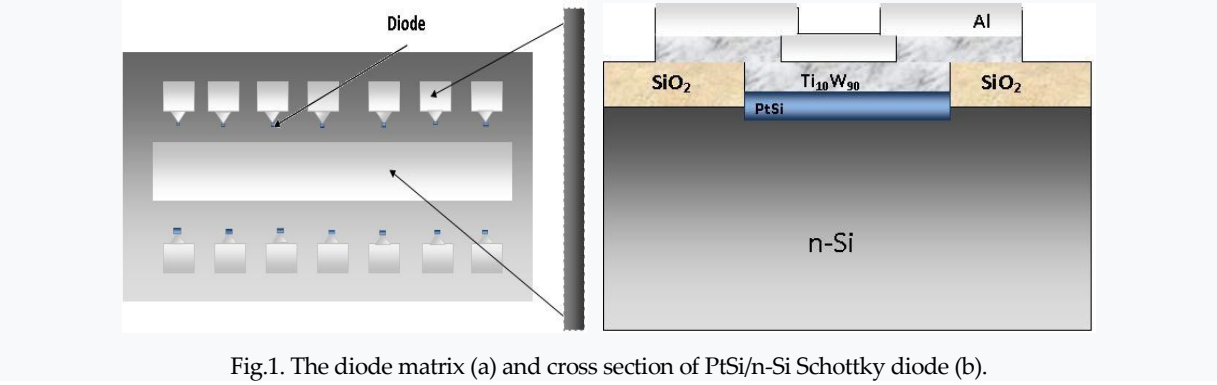

Fig.1. The diode matrix (a) and cross section of PtSi/n-Si Schottky diode (b).

The dependences of the dielectric properties, conductivity, resistance and power dissipation of a PtSi/n-Si Schottky diode on the amplitude of the alternating voltage were obtained as a result of measurements using an HP 4192A low-frequency impedance analyzer and an external pulse generator.

A bias voltage (-2V ÷ +4V) and an alternating signal (500kHz, 5mV÷$1x10^3$mV) were simultaneously applied to the PtSi/n-Si Schottky diode.

3.Results and Discussion

To study the influence of the amplitude of the alternating signal (Vac) on the dielectric parameters of a PtSi/n-Si Schottky diode, measurements of the capacitance (C) and conductance (G) of the diode were carried out when changing direct (V_{dc}) and alternating voltage (V_{ac}).

It is known that complex permittivity can be described as [18-23]

$$\varepsilon^* = \varepsilon' - i\varepsilon'' \quad (1)$$

where real (ε′) and imaginary parts (ε″) of complex permittivity, i is the imaginary root of -1.

At admittance Y^* measurements $C-V$ and $G/\omega-V$, the following relation holds

$$\varepsilon^* = \frac{Y^*}{j\omega C_0} = \frac{C}{C_0} - i\frac{G}{\omega C_{oi}} \quad (2)$$

where C is measured capacitance, G is measured conductance of investigated diode, C_0 is the capacitance of an empty capacitor, ω is the angular frequency ($\omega = 2\pi f$) of the applied electric field.

With the aim of investigation the real (ε') and imaginary (ε″) parts of complex permittivity (ε^*) of PtSi/n-Si(111) Scottky barrier diode have been calculated at different value of alternating voltage (V_{ac}) on the basis of measured C-V and G-V characteristics

$$\varepsilon' = \frac{C}{C_0} = \frac{Cd_i}{\varepsilon_0 A} \quad (3)$$

where d_i is the thickness of the dielectric gap, A = $8x10^{-6}$ cm^{-2} is the rectifier contact area of PtSi/n-Si Schottky barrier diode, ε_0 is the permittivity of free space charge (ε_0 = $8.85 \cdot 10^{-14}$ F/cm).

In the generalized model of the metal–semiconductor contact must be taken into account the presence of thin dielectric gap between contacting materials. In this respect, in the strong accumulation region, the maximal capacitance of the structure corresponds to the dielectric layer capacitance (C_{ac}=C_i=$\varepsilon_i\varepsilon_0 A/d_i$).

By the using measured conductance of PtSi/n-Si Schottky barrier diode at the various amplitudes (V_{ac}) of ac-signal was calculated the imaginary part of the complex permittivity ε″

$$\varepsilon'' = \frac{G d_i}{\varepsilon_0 \omega A} \qquad (4)$$

The loss tangent (tanδ) for PtSi/n-Si Schottky barrier diode can be expressed as

$$tan\delta = \frac{\varepsilon''}{\varepsilon'} \qquad (5)$$

The ac-electrical conductivity (σ_{ac}) for PtSI/n-Si Schottky diodes was calculated by the following equation.

$$\sigma_{ac} = \omega C tan\delta\left({}^{d}/_{A}\right) = \varepsilon'' \omega \varepsilon_0 \qquad (6)$$

Comparing the real and imaginary part of the impedance, the series resistance is given by [24]

$$R_s = \frac{G}{G^2+(\omega C)^2} \qquad (7)$$

Besides, to analyze the dynamics of charge carriers in PtSi/n-Si have been used the complex electric modulus, which is inversely proportional to the complex permittivity [25].

The main advantage of this method is that it suppresses the contribution from electrode polarization, which dominates the permittivity formalism. The real component M' and the imaginary component M'' are calculated from ε′ and ε''.

$$M^* = \frac{1}{\varepsilon^*} = M' + jM'' = \frac{\varepsilon'}{\varepsilon'^2+\varepsilon''^2} + j\frac{\varepsilon''}{\varepsilon'^2+\varepsilon''^2} \qquad (8)$$

It should be noted that the results of research into power dissipation due to dielectric losses are important in the fabrication of new devices.

The power dissipated in the dielectric depends on the amplitude of the alternating signal (V_{ac}) , determine by dielectric losses [14,26-31] and described for device with parallel equivalent circuit (Schottky diodes) as

$$P = V_{ac}^2 \omega C tan\delta \qquad (9)$$

In Fig. 2, 3 and 4 show the change in the real (ε'), imaginary (ε'') parts of the dielectric constant and loss tangent (tan δ) of a PtSi/n-Si diode with a Schottky barrier depending on the bias voltage and the amplitude of the alternating signal (V_{ac}).

As shown in Fig. 2a, Fig. 3a and Fig. 4a, the main parameters characterizing the dielectric properties ε', ε'' and tanδ depend on the bias voltage only in the range of 0-2.0 V at room temperature (T = 300K). At high values of the applied voltage, the values of ε', ε'' reach almost constant values. The studied parameters do not depend on the amplitude of the alternating signal, varying from 5 mV to 1x10^3 mV at a frequency of 500 kHz, with the exception of V_{ac} = 200 mV (Fig. 2b, Fig. 3b and Fig. 4b). It should be noted that when the amplitude of the alternating signal V_{ac} = 200 mV the characteristics differ sharply from others. However, the nature of the dependence remains. Thus, it indicates that at V_{ac} = 200 mV the polarization in PtSi/n-Si Schottky barrier diodes sharply increases.

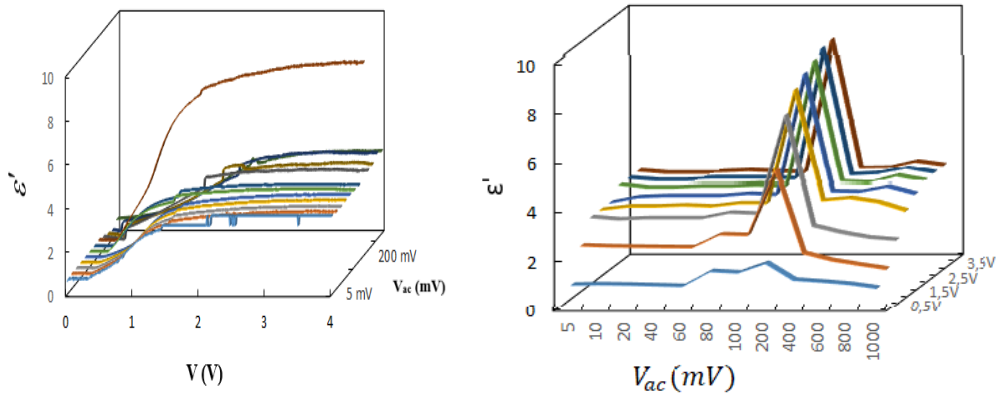

Fig. 2. The dependence of the dielectric constant of PtSi/n-Si Schottky barrier diode: a) on dc-voltage ($\varepsilon' - V$) for various amplitudes of V_{ac} and b) on amplitude of ac-voltage ($\varepsilon' - V_{ac}$) for various applied bias voltage

A sharp increase in ε' indicates an increase in the intensity of polarization, that is, the accumulation of charge at the boundary of regions with different conductivities. The obtained result corresponds to the Maxwell-Wagner theory.

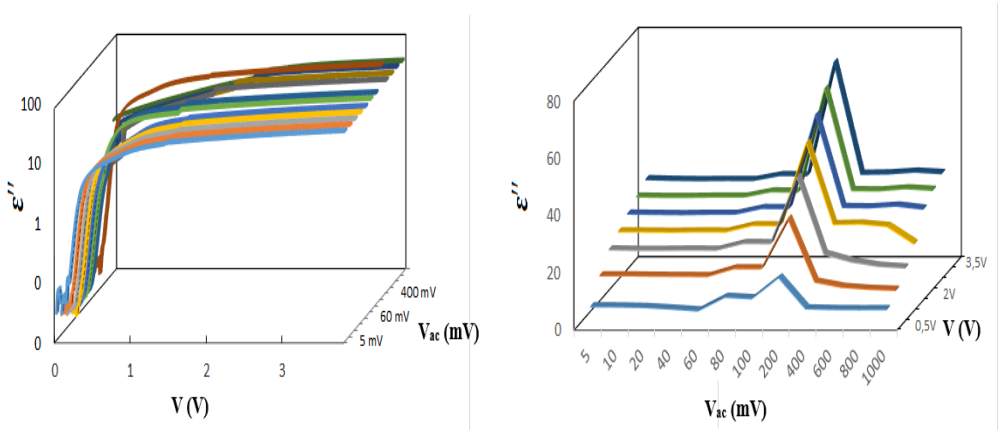

Fig.3. The dependence of the dielectric loss of PtSi/n-Si Schottky barrier diode at room temperature: a) on bias volage ($\varepsilon'' - V$) for various amplitudes of V_{ac} and b) on amplitude of ac-signal (ε''-V_{ac}) for various applied dc- voltage

As can be seen in these figures, the peak values on $\varepsilon'' - V_{ac}$ (Fig. 3b) and $tan\delta$ -V_{ac} (Fig. 4b) observed at V_{ac} =200 mV, increase with increasing dc-voltage, the positions of the peaks do not shift.

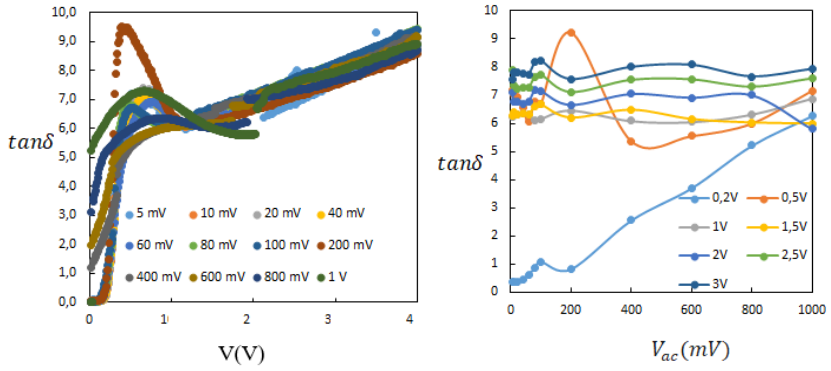

Fig 4. The dependence of tangent loss of PtSi/n-Si Schottky barrier diode at room temperature on: bias voltage a) ($tan\delta - V$) for various amplitudes of V_{ac} and b) on amplitude of alternating signal ($tan\delta$ -V_{ac}) for various applied voltage

The $tan\delta - V$ characteristics have a peak only at V_{ac}=200mV.

The nature of the dependences ε'' and $tan\delta$ on bias voltage and amplitude of alternating voltage, the appearance of the peak and its position depends on polarization, conductivity, surface states, homogeneity of the medium, energy losses, degree of doping, etc. Besides, the capacitance and conductance of diode are extremely sensitive to the interface properties and series resistance. In this case, the contribution of surface states recharging at given frequencies of the alternating signal is of great importance.

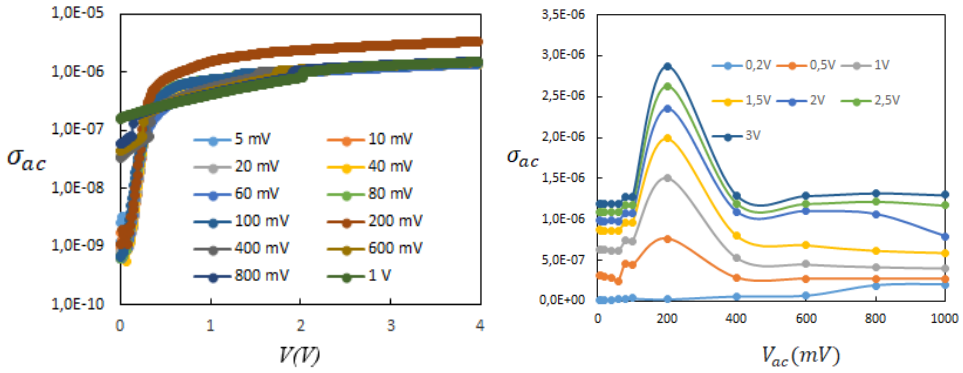

Fig 5. The variations of ac-electrical conductivity (σ_{ac}ac) of PtSi/n-Si Schottky barrier diode at room temperature: a) on dc-voltage ($tan\delta - V$) for various amplitudes of V_{ac} and b) ac-voltage ($tan\delta$ -V_{ac}) for various applied voltage

The behavior of ac-electrical conductivity (σ_{ac}) of the PtSi/n-Si Schottky barrier diode at different voltage and V_{ac} is presented in Fig. 5. It is noticed that the electrical conductivity generally increases with increasing voltage. However, at low and high value of amplitude (V_{ac}) σ_{ac} practically independent on $V_{ac}$with the exception of 200mV.

In the present paper according to a method by Nicollian and Brews [24], the real series resistance of PtSi-nSi Schottky barrier diode was calculated from the $C - V$ and $G - V$ characteristics in strong accumulation region.

The dependence of R_s of investigated diode (PtSi/n-Si) on bias voltage and amplitude of alternating signal (V_{ac}) show in fig.6.

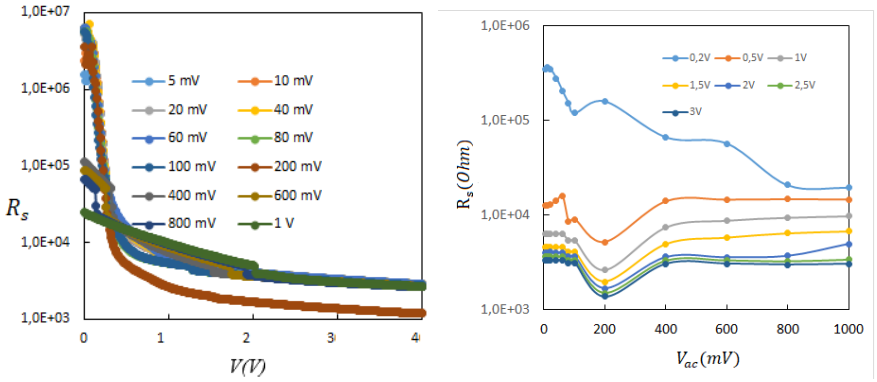

Fig 6. The dependence of the real series resistance R_s of PtSi/n-Si Schottky barrier diode at room temperature (500kHz): a) on dc-voltage ($R_s - V$) for various amplitudes (V_{ac}) and b) on ac-voltage (R_s -V_{ac}) for various applied dc-voltage

By the using real (ε') and imaginary (ε'') parts of complex permittivity have been calculated the dependence of real (M') and the imaginary (M'') parts of electric modulus for PtSi/n-Si Schottky barrier diode on bias voltage and amplitude of alternating signal (Fig.7 and Fig.8)

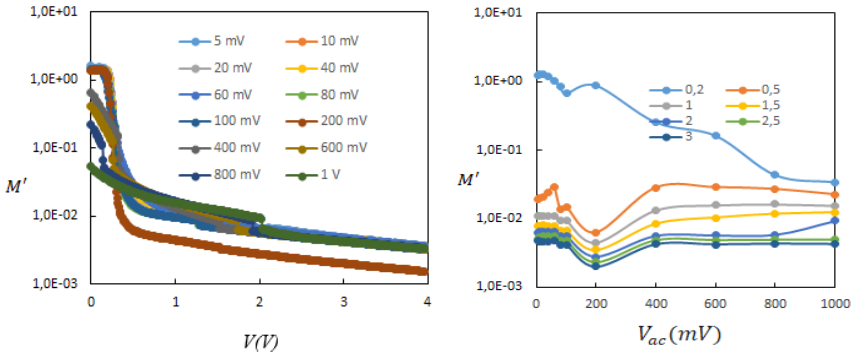

Fig. 7. The dependence of the real part electric modulus (M') of PtSi/n-Si Schottky barrier diode at room temperature on bias voltage: a) $M' - V$ for various amplitudes of V_{ac} and amplitude of alternating signal; b) M' -V_{ac} for various applied voltage

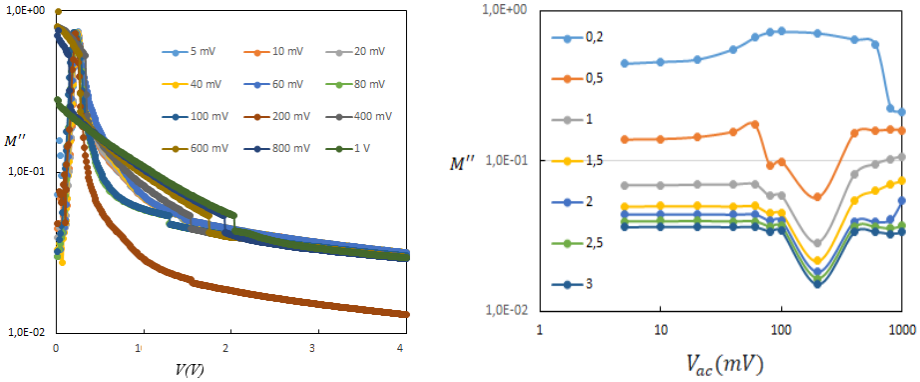

Fig.8. The dependence of the imaginary part of electric modulus (M'') of PtSi/n-Si Schottky barrier diode at room temperature on bias voltage: a) $M'' - V$ for various amplitudes of V_{ac} and amplitude of alternating signal; b) M'' -V_{ac} for various applied voltage

It can be seen from figures 2-8 that all characteristics have features precisely at V=200 mV.

As is know, ε'' is a measure of energy loss and shows how strongly a material absorbs energy from an external electric field. The loss factor ε'' is affected by both dielectric losses and conductivity. The peak in the ε'' dependence and the sharp minimum on $M'' - V_{ac}$ shows an increase in relaxation losses at V_{ac} = 200 mV.

In connection with the aim of the study the power dissipated (P) in the diode PtSi/n-Si was investigated. The dependence $P - V_{ac}$revealed an increase in power dissipation with increasing amplitude of the alternating signal (5mV÷1x10³ mV). In addition, the dependence clearly shows a weak peak at V_{ac} =200 mV (Fig. 9).

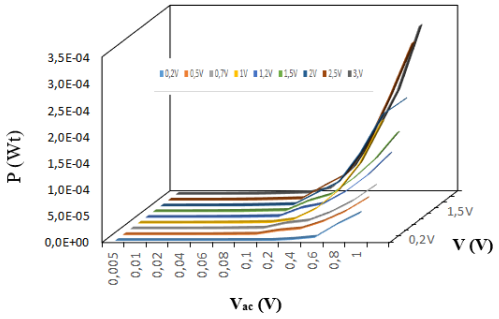

Fig.9. The dependence of the active power dissipated (dielectric losses) (P) in the PtSi/n-Si Schottky barrier diode on the amplitude of ac-signal V_{ac}

The obtained dependence ($P - V_{ac}$) may be due to the heterogeneous structure of depletion layer in PtSi/n-Si Schottky diode. This structure is identical to the Maxwell-Wagner structure of two-layer dielectric [32].

It should be noted that in our previous paper [33], devoted to the study of PtSi/n-Si Schottky barrier diode, the existence of self-assembled patches with different charge carrier concentrations was discovered. The sizes of these spots, similar to quantum wells, were estimated. These patches formed due to hexagonal voids in the crystal structure of Si(111), because the dimensions of these voids allow the penetration of platinum atoms at forming a contact.

We believe that the role of macrorelaxers is played by inhomogeneous sections of the PtSi/n-Si Schottky barrier diode and with the recharging of surface states [4,6]. The density of surfage states (N_{ss}) obtained by the high-low temperature method for the PtSi/n-Si structure revealed the maximum value of N_{ss} about V=200 mV. That is, the N_{ss}values give a wide peak when E_c - E_{ss} = 0,22 eV. Studies in the [33] article showed the maximum loss tangent at 200 mV [10].

So, the features in the dependence parameters on V_{ac} for PtSi/n-Si Schottky barrier diodes revealed that the dissipation power at a voltage of 200 mV is associated with the presence of self-assembled patches in the depletion layer of diode and the maximum density of surface states.

4. Conclusion

The dependence of real (ε') and imaginary (ε″) parts of complex dielectric permittivity and electric modulus (M' , M''), dielectric loss ($tan\delta$), ac-conductivity (σ_{ac}) and series resistance (R_s) on bias voltage (V) and amplitude of alternating signal (V_{ac}) were investigated for PtSi/n-Si Schottky barrier diode. With the increasing of bias voltage from -2V to 4V and amplitude of alternating signal (500kHz) in the range 5mV ÷1x10^{3}mV at room temperature on the all parameters have been observed features only at V_{ac}=200mV. On the dependence of power dissipated on amplitude of alternating voltage revealed the strong dependence and a peak at V_{ac}=200mV also.

The results obtained are in good agreement with previously obtained ones, where the presence of self-organized patches in depletion layer of PtSi/n-Si Schottky barrier diodes with a high doping degree was reported. Inhomogeneous sections of the PtSi/n-Si Schottky barrier diode and the recharging of surface states play a role of macrorelaxers. The value of the alternating signal amplitude ($V_{ac} = 200mV$) causing a sharp change in the parameters corresponds to the maximum value of the density of surface states.

REFERENCES

1. Pellegrini B. Currentvoltage characteristics of silicon metallic silicide interfaces. Solid State Electron, 1975, 18(5): 417 [1].
2. Murarka S P. Silicides for VLSI application. New York: Academic Press, 1983 [2].
3. Sze S.M. Physics of semiconductor devices. New York: John Wiley and Sons, 1981.
4. Buzanyova E.V. Microstructures of integrated electronics. Moscow, Radio i Svyaz, 1990 (in Russian)
5. Poate J M, Tu K N, Mayer J W. Thin films—interdiffusion and reactions. New York: Wiley-Interscience, 1978.
6. Strikha V I. Theoretical bases of metal–semiconductor contact work. Kiev, Naukova Dumka, 1974 (in Russian),
7. Lin J F, Bird J P, He Z, et al. Signatures of quantum transport in self-assembled epitaxial nickel silicide nanowires. Appl Phys Lett, 2004, 85(2): p.281.
8. Hsu H F, Chiang T F, Hsu H C, et al. Shape transition in the initial growth of titanium silicide clusters on Si (111). Jpn. J Appl Physi, 2004, 43(7S): 4541
9. Shaskolskaya M P. Crystallography. Moscow, Visshaya shkola, 1984. (In Russian)
10. Afandiyeva I.M., Bülbül M.M, Altındal S., Bengi S., Frequency dependent dielectric properties and electrical conductivity of platinum silicide/Si contact structures with diffusion barrier/Microelectronic Engineering 93 (2012) p.50–55.
11. Afandiyeva I.M., Dokme I., Altındal S., Bulbul M.M, Tataroglu A. Frequency and voltage effects on the dielectric properties and electrical conductivity of Al–TiW–Pd_2Si/n-Si structures/ Microelectronic Engineering 85 (2008) 247–252.
12. Afandiyeva I.M., Altındal Sh. Temperature dependenced conductivity of PtSi/n-Si Schottky diodes with self-assembled patches/ Conference proceedings Modern Trends in Physics, Baku, 01-03 May, 2019 p.80-84.
13. Afandiyeva I.M, Kuliyeva T.Z., Qojaeva S.M, Abdullayeva L.K. Influence of illumination on dielectric characteristics of Al-TiW-PtSi/n-Si Int. Conference Modern Trends in Physics, 20–22 April 2017, Baku, p.33-36. (In Russian)
14. Oreshkin P.T. Physics of semiconductors and dielectrics/Moskow, Visshaya shkola,1977, 450 p. (in Russian).
15. Afandiyeva I.M, Askerov S.G, Abdullayeva L K, et al. The obtaining

of $AlTi_{10}W_{90}Si$(n) Schottky diodes and investigation of their interface surface states density/ Solid State Electron, 2007, 51: 1096

16. Sakurai Y, Takeda Y, Ikeda S, et al. Electrical resistivity and its thermal coefficient of TiW alloy thin films prepared by two different sputtering systems/ Phys Status Solidi C, 2014, 11(9/10): 1423.
17. Kwak J S, Kang K M, Park M J, et al. Improved thermal stability of GaN-based flip-chip light-emitting diodes with TiW-based diffusion barrier. Sci Adv Mater, 2014, 6(10): 2249.
18. Behzad Barış, Frequency dependent dielectric properties in Schottky diodes based on rubrene organic semiconductor// Physica E: Low-dimensional Systems and Nanostructures, Volume 54, December 2013, Pages 171-176
19. Adem Tataroglu,// Electrical and dielectric properties of MIS Schottky diodes at low temperatures/ 2006, Microelectronic Engineering 83(11):2551-2557, DOI:10.1016/j.mee.2006.06.007
20. Irmak Karaduman Er, Ali Orkun Çağırtekin, Murat Artuç, Selim Acar. Synthesis of Al/HfO_2/p-Si Schottky diodes and the investigation of their electrical and dielectric properties// Journal of Materials Science: Materials in Electronics vol. 32, p.1677–1690 (2021).
21. Ali Orkun Çağırtekin, Ahmad Ajjaq, Özlem Barin and Selim Acar// Bias voltage effect on impedance, modulus and dielectric spectroscopies of HfO_2-interlayered Si-based Schottky diodes at room temperature// Physica Scripta, 2021,Volume 96, Number 11// 115807
22. Naveen Kumar, S. Chand// Effects of temperature, bias and frequency on the dielectric properties and electrical conductivity of Ni/SiO2/p- Si/Al MIS Schottky diodes// 2020 Materials Science Journal of Alloys and Compounds
23. Chen, L. F.; Ong, C. K.; Neo, C. P.; Varadan, V. V.; Varadan, Vijay K. (19 November 2004). Microwave Electronics: Measurement and Materials Characterization. eq. (1.13). ISBN 9780470020456.
24. Nicollian E.H., Brews J.R., MOS Physics and Technology, Wiley, New York, 1982
25. P. B. Macedo, C. T. Moynihan and R. Bose, "The Role of Ionic Diffusion in Polarization in Vitreous Ionic Conductors," Physics and Chemistry Glasses, Vol. 13, 1972, pp. 171-179.

26. Yeh H.J. Radio frequency (RF)/dielectric welding of medical plastics, Joining and Assembly of Medical Materials and Devices, 2013
27. Kotnik Tadej, Miklavcic Damijan. Theoretical evaluation of the distributed power dissipation in biological cells exposed to electric field/ July 2000/ Bioelectromagnetics 21(5):385-394/DOI: 10.1002/1521-186X(200007)21:53.3.CO;2-6
28. Wonseok Shin, Aaswath Raman, and Shanhui Fan/ Instantaneous electric energy and electric power dissipation in dispersive media// ournal of the Optical Society of America B// Vol. 29,Issue 5, pp. 1048-1054, (2012), https://doi.org/10.1364/JOSAB.29.001048
29. Malyshkina O.V., Eliseev A.Yu. Power Dissipation during Dielectric Loop Evolution in PZT Ceramics// Ferroelectrics ,vol. 480, 2015 - Issue 1: Proceedings of the Twelfth European Conference on Applications of Polar Dielectrics (ECAPD-12), p.10-15
30. Rajneesh Talwar, Ashoke Kumar Chatterjee// Estimation of power dissipation of a 4H-SiC Schottky barrier diode with a linearly graded doping profile in the drift region/ 2009, Maejo International Journal of Science and Technology 3(3):352-365
31. Dallas T. Morisette, J.A. Cooper Jr. Theoretical comparison of SiC PiN and Schottky diodes based on power dissipation considerations // 2002, IEEE Transactions on Electron Devices 49(9):1657 – 1664, DOI: 10.1109/TED.2002.801290,
32. A. Chelkowski, Dielectric Physics, Elsevier, Amsterdam, 1980.
33. Afandiyeva I. M., Altındal Ş. Abdullayev L. K., and Bayramova A. İ. Self-assembled patches in PtSi/n-Si (111) diodes// Journal of Semiconductors May 2018/ Vol. 39, No. 5, 054002 -1-7

JOURNAL OF BAKU ENGINEERING UNIVERSITY - PHYSICS
2024. Volume 8, Number 1 *Pages 26-34*

UOT: 666.11.017
Pacs: 62.20. Qp, 61.41. +e, 77.55.+f, 73.50.−h
DOİ: https://doi.org/10.30546/09081.2024.101.5010

A STUDY ON WATER-BASED TRİBOELECTRİC NANOGENERATORS FOR SELF-POWERED MARİNE ENVİRONMENTAL MONİTORİNG SYSTEMS

ORKHAN GULAHMADOV[A]*, MUSTAFA MURADOV[A], HUSEYN MAMEDOV[B], ARZU JAVADOVA[A], ALI MUSAYEV[C], SAID ASLANOV[C] AND JISEOK KIM[A]

[a]*Nano Research Laboratory of the Center for Excellence in Research, Development, and Innovation, Baku State University, Z.Khalilov str. 23, AZ-1148 Baku, Azerbaijan*

[b]*Baku State University, Faculty of Physics, Department of Physical Electronics, Baku, 1148 Azerbaijan*

[c]*Khazar University World School, Baku, 1148 Azerbaijan*

**Corresponding author: Orkhan GULAHMADOV*

ogulahmadov@bsu.edu.az

ARTICLE INFO

Article history:
Received: 2024-10-16
Received in revised form: 2024-10-21
Accepted: 2024-10-25
Available online

Keywords:
triboelectric nanogenerator, polysiloxane, nylon, origami, self-powered
2-4 JEL Classifications codes: O13, N7, P23

ABSTRACT

This study focuses on developing an origami-structured triboelectric nanogenerator (TENG) fabricated from nylon and polysiloxane materials. The origami configuration exhibited a superior energy-harvesting capability compared to conventional single-layer designs. The device's output parameters, including voltage and current, were evaluated manually and under stand-alone operational conditions. The hand-operated TENG achieved a peak voltage of 21 V and a current of 2.8 μA. Under autonomous operation, these values were measured at 8.3 V and 1.04 μA, respectively. The results indicate that both external force and operational frequency have a pronounced effect on enhancing the output performance of the TENG. Wave-driven TENGs (W-TENGs) also demonstrated successful energy harvesting from ocean waves, effectively powering low-energy portable devices. These findings underscore the potential for sustainable energy generation in marine environments, positioning TENGs as a viable solution for self-powered marine environmental monitoring systems.

1. Introduction

In modern times, the growing demand for portable electronic devices—such as smartphones, video cameras, laptops, smartwatches, navigators, and power banks—has significantly influenced daily life, allowing users to engage with technology in a convenient, safe, and efficient manner. This prevalence of devices necessitates reliable and sustainable energy sources to power them. Traditionally, batteries have served as the primary means of electric power supply; however, their limited lifespan and the environmental concerns associated with battery disposal have prompted researchers to explore safer and more sustainable alternatives.

One promising technology that has emerged to meet these energy demands is the triboelectric nanogenerator (TENG) [1-3]. TENGs are versatile devices capable of efficiently harvesting energy from various mechanical sources through the principles of contact electrification and

electrostatics. When two dissimilar materials come into contact and then separate, one material acquires a positive charge while the other acquires a negative charge (Figure 1).

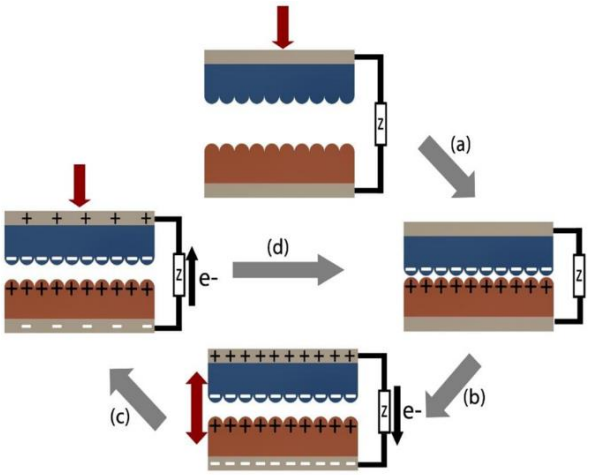

Fig. 1 The mode of operation for contact separation. (a) The pressing phase is when two insulators come into touch with one another due to an external force, creating a triboelectric charge on surfaces. (b) The releasing step causes electron flow between electrodes. (c) A change in the potential difference causes electron backflow when repressing with an external force. (d) The electron flow approaches equilibrium at the point of intimate contact once more is established.

This electrostatic charge remains on the surfaces of the materials as long as they are non-conductive, allowing for an electric current to flow when connected to electrodes [4]. This simple operational mechanism distinguishes TENGs from other energy harvesting systems, enabling them to capture energy from a wide array of sources, including human motion, ocean waves, and wind [5,6].

The efficiency and low production costs of TENGs position them as a significant power source for portable electronic devices. Their broad range of applications has spurred rapid development and innovation, leading to the creation of various structures and TENG-based sensors [5]. These sensors facilitate the acquisition of critical information related to environmental conditions, such as pressure, temperature, humidity, and wind speed, enhancing their usability in everyday life. Moreover, TENGs can effectively harness mechanical and wind energy for applications in military technology, outdoor activities like camping, and scientific research conducted in challenging environments, including mining and mountaineering. In the context of marine environmental monitoring, the increasing demand for sustainable and autonomous energy sources has led to significant interest in developing self-powered systems. Continuous, real-time data collection is critical for assessing and preserving marine ecosystems; however, traditional energy sources such as batteries require frequent maintenance and replacement, especially in remote and harsh ocean environments, limiting their effectiveness. This challenge has spurred interest in renewable energy harvesting technologies, with TENGs emerging as a promising solution [7].

The abundant and continuous motion of ocean waves presents a significant opportunity for energy harvesting, making water-based TENGs a viable candidate for powering autonomous monitoring systems. This study explores the development of a water-based TENG specifically designed for marine environmental monitoring. By leveraging an origami-structured TENG composed of nylon and polysiloxane materials, the research investigates its potential to convert ocean wave energy into usable electrical power. Additionally, the study examines the effects of external force and frequency on the TENG's performance, along with the potential for wave-

driven TENGs (W-TENGs) to power low-energy portable devices in real-world marine environments [8-12].

To enhance the output performance of TENGs, significant research has focused on increasing the contact area of triboelectric materials, which is crucial for optimizing energy conversion efficiency [13]. The development of origami structures that incorporate multiple layers represents a promising approach. By increasing the number of contact surfaces, these designs facilitate the generation of more charge carriers, thereby improving current output and overall power generation.

This research work developed a three-layer origami structure TENG using nylon and polyurethane films. Comparisons were made between electrical measurements of a single-layer TENG and measurements of a three-layer TENG with an origami structure. The obtained electrical measurements show that the TENG with the origami structure yields better results, demonstrating higher voltage and current outputs. Consequently, this leads to an increase in the output power of the triboelectric nanogenerator.

2. Materials and experiment

2.1 Materials and fabrication of triboelectric nanogenerator

In this study, we utilized nylon (specifically, nylon socks made from 100% nylon) and polysiloxane (PS) as triboelectric materials due to their favorable charge-generation properties. The preparation process began with the application of a nylon double-sided adhesive to a pre-made aluminum foil substrate, ensuring good adhesion and stability for the triboelectric components. After applying the adhesive, the assembly was allowed to cure overnight, ensuring that the adhesive bond was strong and effective. The following day, we carefully cut 5x6 cm layers from the adhered nylon material and removed any excess to ensure a clean and uniform interface for charge generation. Simultaneously, we prepared the polysiloxane layer by employing a drop-casting method (Fig. 2a). In this process, a controlled amount of PS was applied onto a separate aluminum foil substrate, forming a uniform film. The drop-casted PS was allowed to dry at room temperature for a full day to ensure complete evaporation of the solvent and proper formation of the film (Fig. 2b). Once the drying process was completed, we also cut 5x6 cm sheets of PS to match the dimensions of the nylon layers.

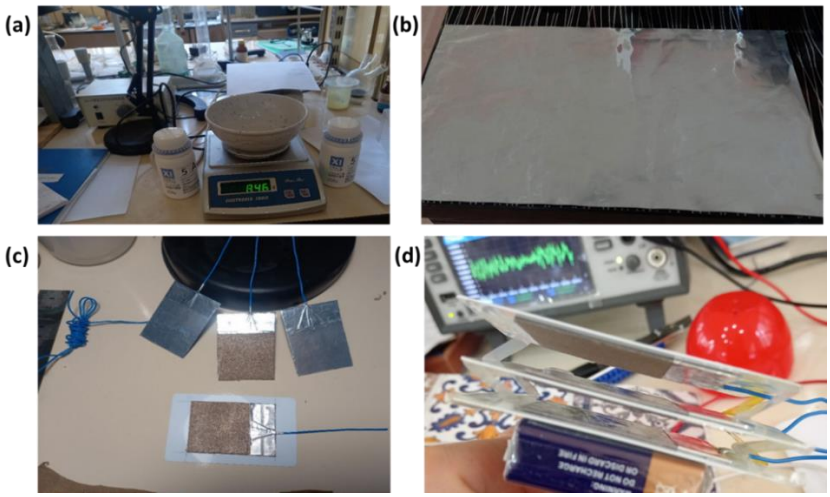

Fig. 2 a) polysiloxane solution; b) investigating of PS films by using drop casting method; c) triboelectric materials; d) prototype of origami structured TENG

The TENG was then assembled by combining the nylon and PS films with the aluminum foil, creating a layered structure that capitalizes on the triboelectric effect. The interaction between the nylon and polysiloxane surfaces is essential for effective charge transfer, with each material contributing to the overall charge generation mechanism. The resulting triboelectric materials (Fig. 2c), with their unique origami-inspired design, are illustrated in Figure 2d.

2.2 Measurement of output performance of TENG

Nylon and PS are used as dielectric materials and aluminum foil as metal electrodes in the manufacture of triboelectric nanogenerators. Nylon and PS are considered good triboelectric pairs because of their distance from each other in the triboelectric series [14]. Samples of both materials measuring 5x6 cm are cut and glued to the pre-prepared Al foil using double-sided glue. Tests on a triboelectric nanogenerator based on PS and nylon materials were performed using a digital multimeter (DMM6500 6-1 / 2 digit multimeter, Keithley). Temperature and relative humidity during the analysis were 30 ° C, and 53%, respectively.

3. Results and discussion

This research utilized nylon and polysiloxane (PS) materials to craft a TENG characterized by its innovative origami-inspired structure. We assessed the performance of the water-based triboelectric nanogenerator (W-TENG) through comprehensive testing and analysis using a digital multimeter (DMM). Our investigation focused on how the output parameters of the W-TENG, including voltage and current, vary with frequency and applied force (Figure 3). To evaluate the efficiency and functionality of the W-TENG, we measured various electrical parameters under different conditions. As shown in Fig. 3, it was observed that increasing the amplitude of the external force from F=0.3 N to 1 N led to a substantial rise in the voltage output of the W-TENG, from U=1.3 V to 10 V (Fig. 3a). Simultaneously, the current increased from I=0.2 μA to 1.54 μA (Fig. 3b). Figure 3c illustrates the relationship between the maximum values of voltage and current intensity of the W-TENG and the applied force.

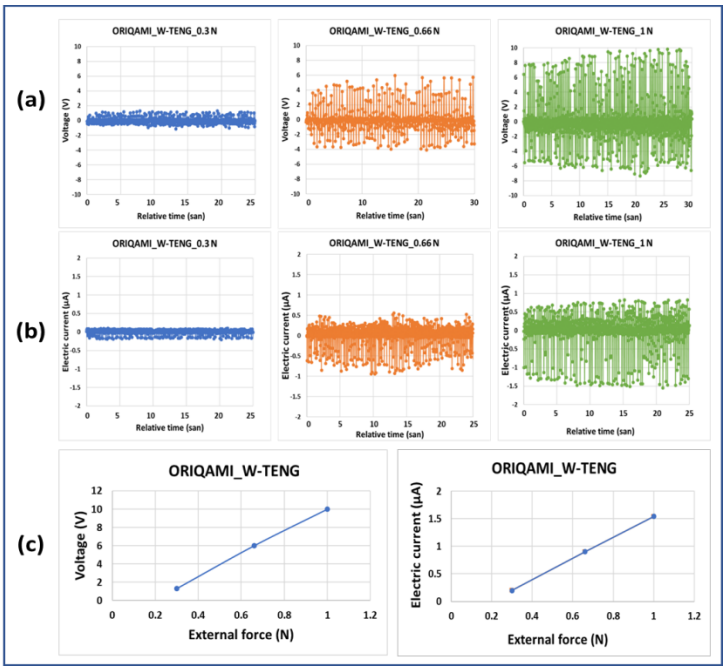

Fig. 3 External force dependence graphs of output parameters of origami-structured W-TENGs: a) Voltage-time dependence of W-TENG; b) Current-time dependence of W-TENG; c) Force dependence of maximum values of voltage and current of W-TENG

These results clearly demonstrate that varying the amplitude of the external force significantly affects the output parameters of the W-TENG. This strong correlation can be attributed to the enhanced interaction between the materials in the W-TENG, specifically nylon and PS . When the external force is increased, these materials come into more extensive contact with each other, resulting in a larger contact area. This increased contact area plays a crucial role in boosting the charge transfer process, as a greater number of charge carriers are generated on the surface during contact. The underlying mechanism driving this phenomenon is based on triboelectric effects and contact electrification principles. As the force applied to the TENG grows, the friction between the contacting materials intensifies, which leads to more significant charge generation.

In TENGs, the effectiveness of energy conversion is highly dependent on the surface interaction of the materials involved. Enhanced surface interaction not only increases the charge density on the contact surfaces but also improves the efficiency of charge separation when the two materials come apart. This separation creates an electric potential difference, resulting in a higher voltage output. The relationship between the output parameters and contact area is critical; as the contact area increases, there is a corresponding rise in the density of static charges on the surface. This phenomenon is a direct result of the triboelectric effect, where the transfer of electrons occurs due to the frictional contact between dissimilar materials. Consequently, a larger contact area not only increases the quantity of generated charges but also enhances the overall efficiency of the energy harvesting process.

Moreover, the greater mechanical deformation due to the increased force also contributes to the efficiency of the TENG. When subjected to higher external forces, the material's structural flexibility allows it to bend or compress more, promoting even more substantial charge transfer through repeated contact and separation cycles. This dynamic response of the TENG to varying forces is critical for optimizing its performance in energy harvesting applications.

As shown in Figure 4, the variation of the TENG's output parameters as a function of frequency exhibited a trend closely resembling that observed with changes in external force. Specifically, as the wave frequency increased from 1 Hz to 3 Hz, the voltage output of the W-TENG rose significantly, from 6.9 V to 11 V (Fig.4a), while the current output increased from 0.6 μA to 1.47 μA (Fig.4b). Figure 4c illustrates the relationship between the maximum values of voltage and current intensity of the W-TENG and the frequencies.

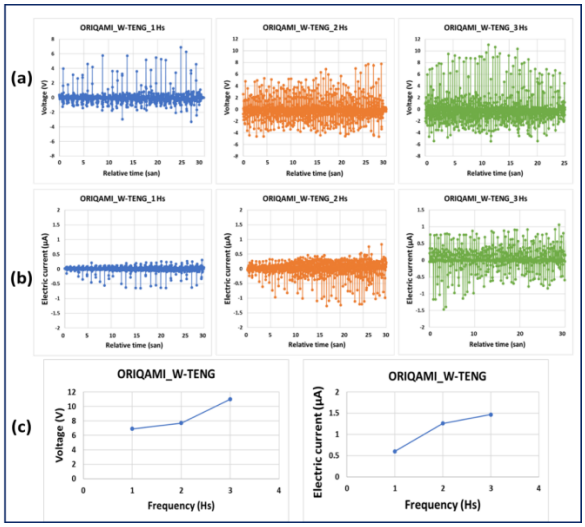

Fig. 4 Frequency dependence graphs of output parameters of origami-structured W-TENGs:
a) Voltage-time dependence of W-TENG; b) Current-time dependence of W-TENG;
c) Frequency dependence of maximum values of voltage and current of W-TENG

This upward trend in output parameters is indicative of a strong correlation between the applied frequency and the TENG's energy generation capabilities. The underlying mechanism for this frequency-dependent increase in output parameters can be attributed to the intensified material contact at higher frequencies. As the frequency of the applied force rises, the nylon and PS materials undergo more frequent cycles of contact and separation. These rapid cycles of interaction lead to a greater accumulation of triboelectric charges on the surface of the materials, thereby enhancing the overall charge density available for energy conversion. This effect is primarily due to the dynamic behavior of the triboelectric layers during high-frequency oscillations. With each successive contact, the speed of charge transfer and separation increases, causing a more efficient buildup of surface charges. As a result, the electric potential difference generated between the layers becomes larger, which directly translates to a higher voltage output. Concurrently, the faster charge movement also boosts the current output of the W-TENG, as a greater number of electrons are displaced per unit of time.

Additionally, the increased frequency amplifies the mechanical vibrations within the TENG structure. These vibrations cause more intense mechanical deformation of the triboelectric materials, thereby maximizing the contact area during each cycle. With a larger effective contact area, more charges can be generated and separated, leading to enhanced triboelectric performance. This mechanical amplification effect explains why the TENG exhibits a more pronounced response at higher frequencies, which is crucial for optimizing its efficiency in various energy-harvesting applications. At higher frequencies, the time interval between each contact-separation event is reduced, meaning that the system experiences less charge leakage between cycles. This reduction in charge dissipation ensures that the charges accumulated on the surface are more effectively utilized in generating electrical output, thereby improving the TENG's overall energy conversion efficiency.

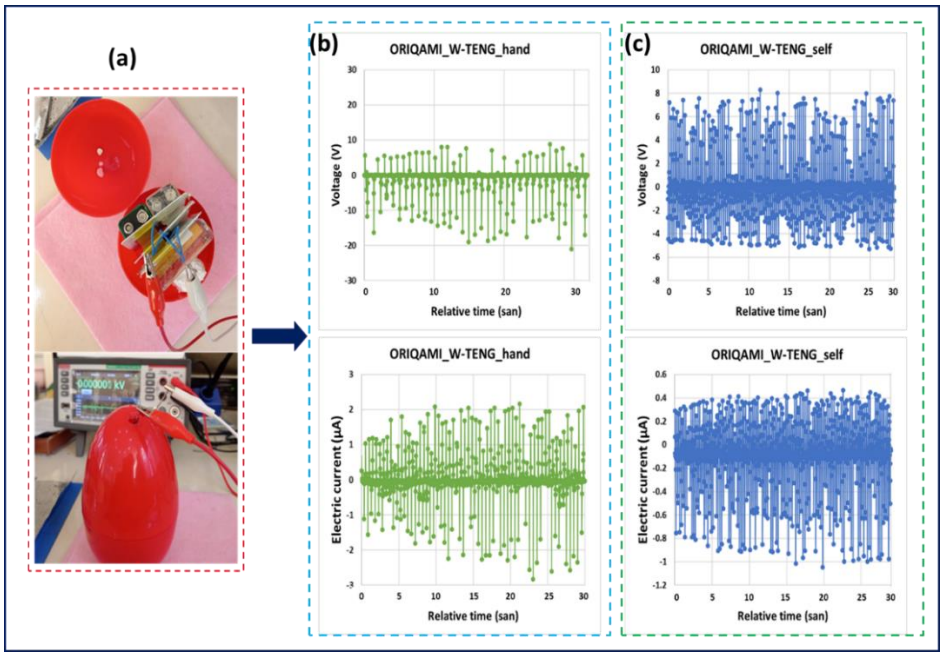

Fig. 5 a) Practical operation of the W-TENG; b) W-TENG voltage and current versus time graphs (manual case); c) W-TENG voltage and current versus time graphs (self-powered case)

Experiments were conducted on the W-TENG prototype, fabricated as depicted in Figure 5, to evaluate its performance under different operating conditions. The output parameters of the

W-TENG, specifically voltage and current, were systematically tested under both manual operation and self-powered system conditions. In the manual operation mode, the maximum voltage achieved by the TENG reached 21 V, with a peak current of 2.8 μA (Fig.5b). Under the self-powered (real mode) conditions, the maximum voltage and current values were 8.3 V and 1.04 μA, respectively (Fig.5c). These results clearly demonstrate the significant influence of external force and frequency on the enhancement of the TENG's output performance. The higher voltage and current values observed during manual operation can be attributed to more controlled and forceful interactions between the triboelectric layers, which lead to an increased contact area and more effective charge transfer. Conversely, in the self-powered mode, the relatively lower output is likely due to the variable and less intense force applied during natural operational cycles, which nonetheless still generates sufficient energy for low-power applications.

Moreover, the study highlights the effectiveness of W-TENGs in harvesting energy from oceanic wave motion, showcasing their potential for sustainable energy generation in marine environments. Figure 6 illustrates the potential practical applications of these W-TENGs. These W-TENGs were able to successfully convert mechanical energy from ocean waves into electrical energy, which was sufficient to power portable electronic devices (Figure 6). This capability underscores the feasibility of deploying TENGs as reliable and eco-friendly energy solutions for offshore and marine-based applications. The successful implementation of wave-driven TENGs opens new avenues for renewable energy technologies, particularly in harnessing ambient energy from natural sources like ocean waves. The robust energy conversion mechanism of TENGs, based on the principles of triboelectric and electrostatic induction, makes them well-suited for applications in remote or underwater environments where traditional energy sources are not viable.

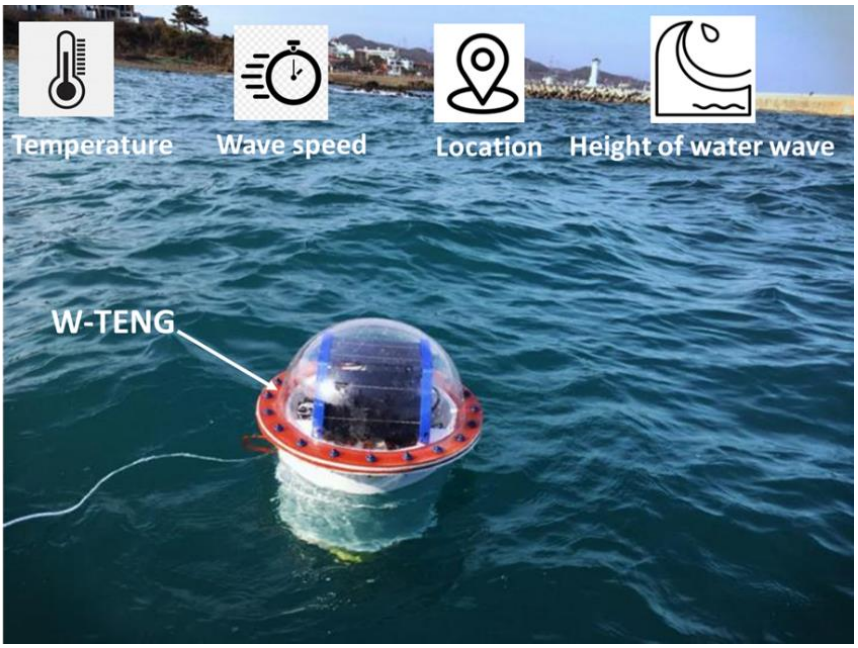

Fig. 6 Application areas of W-TENGs

Furthermore, the scalability of TENG systems presents an opportunity to integrate these devices into larger networks for distributed energy harvesting, contributing to the development of self-sustaining power grids in marine and coastal regions.

4. Conclusion

In this study, we explored the performance of a wave-driven triboelectric nanogenerator (W-TENG) utilizing nylon and polysiloxane (PS) materials, designed with an innovative origami-inspired structure. Through comprehensive testing, we investigated the effects of varying external force and frequency on the W-TENG's output parameters, such as voltage and current. The results showed a significant enhancement in the energy generation capabilities of the W-TENG as both the amplitude of the applied force and the frequency increased. These improvements were primarily attributed to the increased contact area between the triboelectric layers, leading to a more efficient charge transfer and a greater accumulation of surface charges. Our findings highlight the critical role of mechanical deformation and dynamic interactions in optimizing the performance of the W-TENG. The frequency-dependent behavior demonstrated that higher frequencies lead to intensified material contact and rapid cycles of charge transfer, which contribute to improved voltage and current outputs. Additionally, the successful performance of the W-TENG under manual and self-powered conditions further validated its versatility in different operational modes. In conclusion, the W-TENG's innovative design and the successful implementation of wave-driven energy harvesting underscore its potential as a promising technology for renewable energy generation. The correlation between the applied force, frequency, and output performance of the TENG points to a pathway for optimizing its efficiency, making it suitable for a range of applications from portable electronic devices to larger-scale marine energy systems. Future developments in material engineering and structural design could further improve the efficiency and scalability of TENGs, solidifying their role in advancing sustainable energy solutions in diverse environments.

Acknowledgments

We would like to thank Lala Gahramanli, who is the leading researcher of the Nano research laboratory in the Excellence Center of Research, Development, and Innovation of Baku State University for supporting the experimental part.

Conflict of interest

On behalf of all authors, the corresponding author states that there is no conflict of interest.

REFERENCE LIST

1. Niu, Simiao, and Zhong Lin Wang. "Theoretical systems of triboelectric nanogenerators." Nano Energy 14 (2015): 161-192.
2. Cheng, Tinghai, Jiajia Shao, and Zhong Lin Wang. "Triboelectric nanogenerators." Nature Reviews Methods Primers 3, no. 1 (2023): 39.
3. Kim, Weon-Guk, Do-Wan Kim, Il-Woong Tcho, Jin-Ki Kim, Moon-Seok Kim, and Yang-Kyu Choi. "Triboelectric nanogenerator: Structure, mechanism, and applications." ACS nano 15, no. 1 (2021): 258-287.
4. Wu, Changsheng, Aurelia C. Wang, Wenbo Ding, Hengyu Guo, and Zhong Lin Wang. "Triboelectric nanogenerator: a foundation of the energy for the new era." Advanced Energy Materials 9, no. 1 (2019): 1802906.
5. Gulahmadov, Orkhan, Mustafa B. Muradov, and Jiseok Kim. "Gait analysis by using electric signals from a triboelectric nanogenerator." Engineering Research Express. 2022, v. 4, p. 1-8.
6. Wang, Yang, Ya Yang, and Zhong Lin Wang. "Triboelectric nanogenerators as flexible power sources." npj Flexible Electronics 1, no. 1 (2017): 10.
7. Zi, Yunlong, Jie Wang, Sihong Wang, Shengming Li, Zhen Wen, Hengyu Guo, and Zhong Lin Wang. "Effective energy storage from a triboelectric nanogenerator." Nature communications 7, no. 1 (2016): 10987.
8. Shen, Fan, Zhongjie Li, Hengyu Guo, Zhengbao Yang, Hao Wu, Min Wang, Jun Luo, Shaorong Xie, Yan Peng, and Huayan Pu. "Recent advances towards ocean energy harvesting and self-powered applications based on triboelectric nanogenerators." Advanced Electronic Materials 7, no. 9 (2021): 2100277.
9. Song, Changhui, Xiao Zhu, Maoli Wang, Ping Yang, Linke Chen, Le Hong, and Weicheng Cui. "Recent advances in ocean energy harvesting based on triboelectric nanogenerators." Sustainable Energy Technologies and Assessments 53 (2022): 102767.
10. Shan, Bingqiang, Tengtian Ai, and Kai Wang. "Triboelectric Nanogenerator for Ocean Energy harvesting: a review of technological advances and future perspectives." International Journal of Electrochemical Science (2024): 100694.
11. Matin Nazar, Ali, King-James Idala Egbe, Azam Abdollahi, and Mohammad Amin Hariri-Ardebili. "Triboelectric nanogenerators for energy harvesting in ocean: A review on application and hybridization." Energies 14, no. 18 (2021): 5600.
12. Xu, Yuhong, Weixiong Yang, Xiaohui Lu, Yanfei Yang, Jianping Li, Jianming Wen, Tinghai Cheng, and Zhong Lin Wang. "Triboelectric nanogenerator for ocean wave graded energy harvesting and condition monitoring." ACS nano 15, no. 10 (2021): 16368-16375.
13. Jiseok Kim., Orkhan Gulahmadov., Mustafa B. Muradov. Enhancement of performance of triboelectric generators by introduction of micro- and nano-structures on triboelectric films. Journal of Materials Science: Materials in Electronics. 2021, v. 32, p. 24661–24680.
14. Shanbedi, Mina, Haleh Ardebili, and Alamgir Karim. "Polymer-based triboelectric nanogenerators: Materials, characterization, and applications." Progress in Polymer Science (2023): 101723.

JOURNAL OF BAKU ENGINEERING UNIVERSITY - PHYSICS

2024. Volume 8, Number 1 ***Pages 35-42***

UDC: 541.64:539.26:537.529
PACS: 541.183.539.26
DOI: https://doi.org/10.30546/09081.2024.101.5012

EFFECT OF γ-RADİATİON ON DİELECTRİC PROPERTİES OF HDPE- α-Al_2O_3 NANOCOMPOSİTES

NABIYEVA A.N., GULIYEV M.M., ISMAILOVA R.S.

Institute of Radiation Problems of SEM
aysel.nabiyeva21@gmail.com

ARTICLE INFO

Article history
Received: 2024-10-08
Received in revised form: 2024-10-16
Accepted: 2024-10-14
Available online

Keywords:
electric modulus,
dielectric properties,
HDPE,
relaxation

ABSTRACT

Dielectric properties of high-density polyethylene/ α-Al_2O_3 (HDPE+ α-Al_2O_3) composite films in the temperature range of 20°–110℃ and in the frequency range of 25–10^6 Hz before and after irradiation have been reported. HDPE matrix may result in changes to the dielectric properties, conductivity, and relaxation behavior. Therefore, investigating the electric modulus as a function of frequency and temperature in this composite system is essential for unraveling the underlying mechanisms and potential applications in electrical devices. The samples were irradiated by means of γ-rays from 0 up to 200 kGy. The experimental dielectric data have been analyzed with electric modulus formalism. The electric modulus representation shows well-defined relaxation peaks.

ВЛИЯНИЕ Г-ОБЛУЧЕНИЯ НА ДИЭЛЕКТРИЧЕСКИЕ СВОЙСТВА НАНОКОМПОЗИТОВ ПЭВП **+A-AL_2O_3**

АННОТАЦИЯ

Представлены диэлектрические свойства композитных пленок полиэтилена высокой плотности/α-Al_2O_3 (ПЭВП+ α-Al_2O_3) в интервале температур 20°–110°C и в диапазоне частот 25–10^6 Гц до и после облучения. Образцы облучались γ-лучами от 0 до 200 кГр. Матрица ПЭВП может привести к изменениям диэлектрических свойств, проводимости и релаксационного поведения. Следовательно, исследование электрического модуля как функции частоты и температуры в этой сложной системе имеет важное значение для раскрытия основных механизмов и потенциальных применений в электрических устройствах. Экспериментальные диэлектрические данные проанализированы формализмом электрического модуля. Представление электрического модуля показывает четко определенные пики релаксации.

***Ключевые слова*:** электрический модуль, диэлектрические свойства, ПЭВП, релаксация,

YSPE+A-AL_2O_3 NANOKOMPOZITLƏRININ DIELEKTRIK XASSƏLƏRINƏ Γ-ŞÜALANMANIN TƏSIRI

XÜLASƏ

Yüksək sıxlıqlı polietilen/α-Al_2O_3(YSPE+α-Al_2O_3) kompozitlərinin şüalanmadan əvvəl və sonra 20°–110°C temperatur diapazonunda və 25–10^6 Hs tezlik diapazonunda dielektrik xassələri məruzə edilmişdir. YSPE matrisi nümunənin dielektrik xassələrində, keçiriciliyində və relaksasiya davranışında dəyişikliklərə səbəb ola bilər. Buna görə də, bu mürəkkəb sistemdə elektrik modulunun tezlik və temperature asılılığını öyrənmək elektrik cihazlarında əsas mexanizmləri və potensial tətbiq sahələri aşkar etmək üçün vacibdir. Nümunələr 0-dan 200 kGy-ə qədər γ-şüaları vasitəsilə şüalandırılmışdır. Eksperimental dielektrik məlumatları elektrik modulu formalizmi ilə təhlil edilmişdir. Elektrik modulunun təsviri yaxşı müəyyən edilmiş relaksasiya piləri göstərir.

Açar sözlər: elektrik modulu, dielektrik xassələri, YSPE, relaksasiya

Introduction:

Polymer composite materials are widely used in microelectronics, electromagnetic compatibility, electromagnetic interference protection, and acoustoelectronics, as insulating systems for high-voltage applications, such as: cables, generators, motors, cast resin dry-type transformers [1]. The electrical and mechanical properties of polymers can be modified by adding inorganic nanofillers. Incorporation of nanosized particles improves the electrical and dielectric properties of polymers. Nanosized particles are more attractive because of the interesting properties that arise from the dimensions associated with the large surface area. The choice of the type and nature of micro- and nanoparticles used as fillers is determined by the given electrical, mechanical [2,4] and thermal [5,6] properties of the composite material. The introduction of nano-alumina oxide into the HDPE matrix may result in changes to the dielectric properties, conductivity, and relaxation behavior. Therefore, investigating the electric modulus as a function of frequency and temperature in this composite system is essential for unraveling the underlying mechanisms and potential applications in electrical devices. There are various methods to understand the dynamics of polymer composite materials. The method of dielectric spectroscopy is a good tool for studying the characteristics of materials. It should be noted that within the framework of the development of new polymer composite materials, it is necessary to have information about the dispersion of the real ε′ and imaginary ε″ parts of the complex dielectric conductivity, the temperature and frequency dependences of the tangent of the dielectric loss angle, and the basic laws of structural relaxation within the framework of the introduction of micro- and nanofillers into the polymer. The study of the electric modulus in polymer nanocomposites has gained significant attention due to its potential applications in various technological fields. In this context, the focus of our investigation is on the electric modulus of high-density polyethylene (HDPE) reinforced with nano-alumina oxide. Nano-alumina oxide (α-Al_2O_3), with its unique electrical and mechanical properties, holds promise for enhancing the electrical performance of polymers [7].

The irradiation of polymeric materials with ionizing radiation (gamma rays, X rays, accelerated electrons, ion beams) leads to the formation of very reactive intermediates products (excited states, ions and free radicals), which result in rearrangements and/or formation of new bonds. It is well known that irradiation enhance the electrical conductivity in insulating polymers. All materials have been found to break down at very high radiation doses, however, the range of doses under which a given polymer will maintain its desirable properties depends greatly on the chemical structure of the polymers. Indeed, below the destructive level of exposure, radiation treatment can impart many benefits and enhance properties of commercial value.

Therefore, in the present research, the frequency and temperature dependences of electrical modulus of the composites based on high-density polyethylene containing nanoparticles of α-Al_2O_3 before and after irradiation were experimentally studied to find the possibilities of controlled change in dielectric properties of composite materials. This article aims to provide a comprehensive analysis of the electric modulus in the HDPE/ α-Al_2O_3 nanocomposite system.

Experimental

As a polymer matrix powdered PE2NT11-285D high-density polyethylene (Russia, Kazan) with melting point of 130°C, and a density of 947g/m3 was selected. The choice of HDPE (particle sizes of no more than 300μm) as the matrix was mostly based on the high dielectric properties and process ability of the material. α-Al_2O_3 (Sky Spring Nanomaterials, Inc. Houston United States) with partical size d=40nm, dielectric permeability of ε≈10, and a density of 3,89g/cm3 was used as a filler.

Film samples of unfilled HDPE and composites based on it were prepared using a process flow sheet involving the following procedures:

– Mixing powders HDPE and α-Al_2O_3 to a visual uniform state in a porcelain mortar.

– Pressing a homogenous mixture of component powders in a hydraulic press with heated plates at a pressure of 15MPa with holding at a temperature of 130°C for 5 min, and obtaining samples of composites in the form of discs with a diameter of 20mm and a thickness of about 90-110nm.

–To ensure reliable electrical contact between the sample and the grounded stainless steel electrodes, pressing on the surface of the electrode made of a thin aluminum foil with a thickness of 7μm, followed by cooling in a water-ice mixture (quenching mode).

Thus, 0-3 composites containing 0÷10vol%α-Al_2O_3 in the HDPE matrix were prepared.

All concentrations given in this study are volumetric. The composite manufacturing mode allows one to obtain repeated electrophysical parameters for the bulk of the samples at the same concentration. Samples that had parameters different from the parameters of the main group (their number was small) were not taken into account in the analysis.

Dielectric spectroscopy analysis of the virgin and gamma irradiated specimens was carried out through a broadband dielectric impedance spectroscopy analyze for understanding the variation of dielectric constant (ε) and dielectric loss (tanδ) of the sample over a wide range frequency and temperature. The analysis of the behavior of the complex electric module was used to obtain additional information and to solve the usual difficulties associated with the influence of the nature of the electrodes, ohmic contact and the effects of space charge injection, so that the real and imaginary parts of the dielectric conductivity "hide" the relaxation in the frequency dependence of the imaginary parts of the dielectric conductivity. The complex electric modulus is defined by the equation M*.

$$M^* = \frac{1}{\varepsilon} = \frac{1}{\varepsilon' - j\varepsilon'} = \frac{\varepsilon'}{\varepsilon'^2 + \varepsilon''^2} + \frac{\varepsilon''}{\varepsilon'^2 + \varepsilon''^2} = M' + j$$

In a low-conductivity system, the rapid increase in conductance at very low frequency is due to electrode polarization, and the effect of electrode polarization can completely mask the low-frequency relaxation. The "electrical modulus" formalism is used to study the dielectric relaxations to remove the electrode polarization effect and resolve the low-frequency relaxation. The electrical module is determined by the following formula

$$M' = \frac{\varepsilon'}{\varepsilon'^2 + \varepsilon''^2}$$

$$\frac{\varepsilon''}{\varepsilon'^2 + \varepsilon''^2}$$

The materials were examined using parallel plate capacitors in a two electrodes system in the equivalent circuit of a resistor and a capacitor connected in parallel in a frequency range of 25-10^6Hz at temperatures of 30-120°C and a measuring voltage amplitude of U=1V, using a special shielded and grounded heated "sandwich" measuring cell with a system of a measuring and potential electrode with a diameter of 14 and 20mm, respectively. Temperature measurements were conducted at a frequency of 1kHz. The samples were placed in the measuring cell with pressure exerting stainless steel electrodes. The temperature of sample was controlled intelligent digital temperature controller using a CH-B702 type (China). The centering of the electrodes was provided by a special mandrel in a heated chamber. The distance between the electrodes was determined by the thickness of the test samples. The measurements of capacitance C, dielectric loss tangent tanδ were conducted in a direction perpendicular to the plane of compression of the samples using an E7-20 broadband precision immittance meter. The accuracy of measurement is within 2-5%.

Studies of the effect of filler concentration and of gamma irradiation of HDPE and composites based on it before and after exposure to these factors. The irradiation of nanocomposites were carried out at room temperature by γ– exposure at a dose rate of 5,65 kGy in an irradiator MRX-γ-30 provided with (^{60}Co) sourse. HDPE film and composite samples were irradiated to absorbed doses D=50 and 200kGy.

Discussion

Modulus spectra are frequently used for characterization of nanodielectric because these spectra are independent of electrode polarization effect, electrode material and the adsorbed impurities, and only give the bulk response of the dielectric material [8]. Fig 1. shows the real and imaginary parts of the electric modulus respectively obtained through equation (2) and (3) as a function of frequency for different volume percentage (up to 10%) of α-Al_2O_3 in different doses (0 kGy, 50 kGy,200 kGy). Measurements were made in the 25-10^6Hz frequency range, at room temperature for examined systems is presented. It can be seen that Fig1a the value of M′ increase with frequency up to 2*10^5Hz (for pure HDPE from 0.31 to 0.34, for HDPE+ 3%α-Al_2O_3 composites from 0.30 to 0.32, for HDPE+ 10%α-Al_2O_3 from 0.27 to 0.30), then deacrease to the end of frequency scale. As expected, the real part of electric modulus of HDPE and HDPE+ α-Al_2O_3 nanocomposites decrease with increase α-Al_2O_3 content: for 3% M′=0.32 and 10% M′=0.33. But value of M′ for 1% and 5% nanocomposites higher than pure HDPE(for 1% M′=0.33, for 5% M′=0.34)

After 50 kGy exposure dose value of M′ decrease than 0 kGy irradiation for all tested composite system. The reduction in the values of M′ with increasing dose results from the increase in the mobility of the polymer segment and charge carriers [8]. It is clearly seen that the real part of electric modulus increases slowly up to 10^3Hz, then increases high rate in comparison previous frequencies up to 2*10^5Hz and obtaion maximum value then decrease end to the frequency scale. The value of M′ decreases with an increase in volume content α-Al_2O_3 in the base mixture as a result of increase of the real part of complex dieletric permittivity and nature of all curves are similar. For all the studied composite samples there is a transition from low values to high ones, which implies the relaxation process. The value of M′ for pure HDPE decreases 1.76 times (from 0.300 to 0.176) after 50 kGy irradiation. The maximum value of M′ for pure HDPE is 0.2.

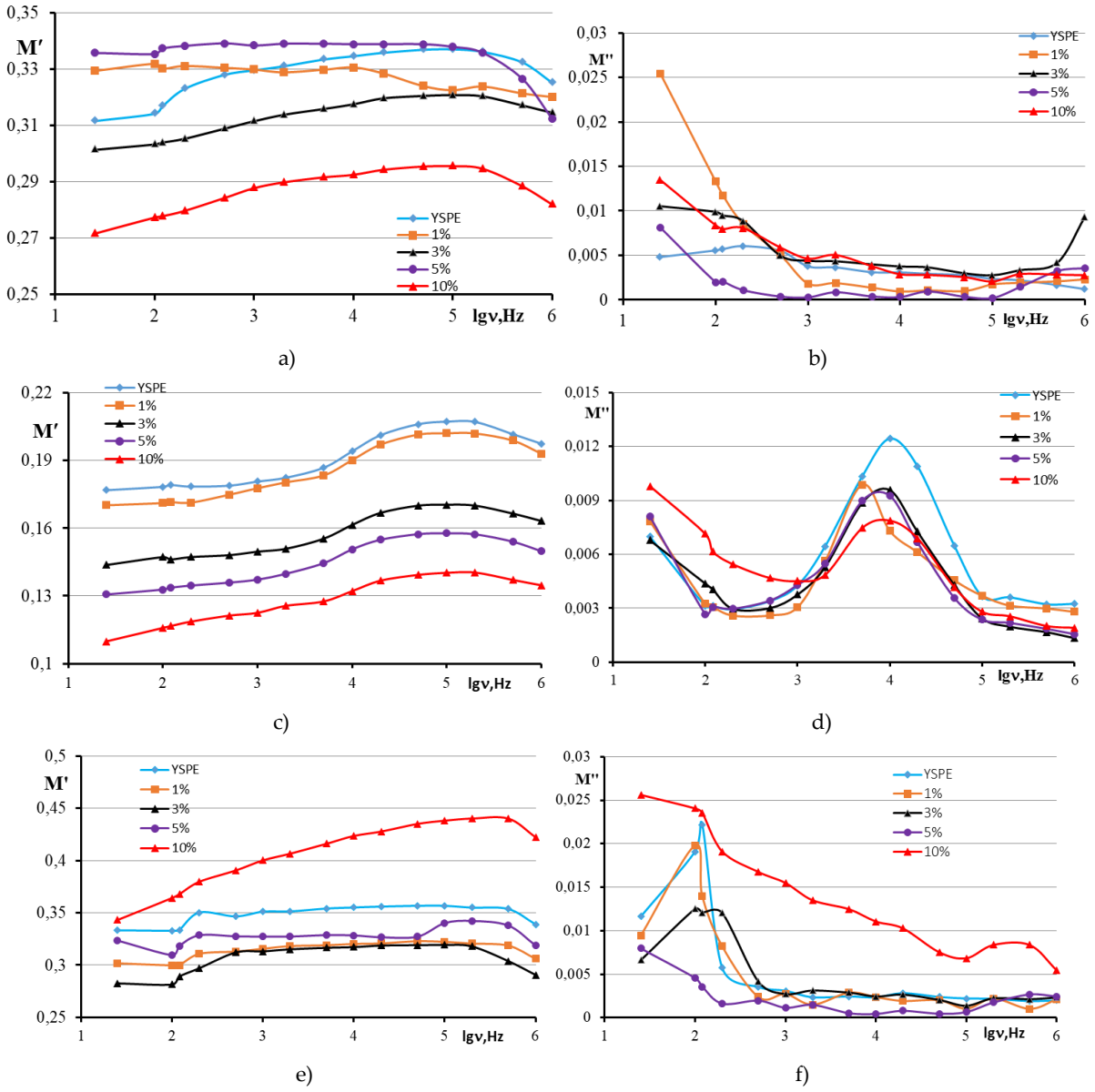

Fig.1. Frequency dependence of real and imaginary parts of electric modulus of HDPE+ x%α-Al_2O_3 at different radiation doses:a,b-0kGy;c,d-50kGy; e,f-200kGy.

At 200 kGy exposure dose value of the real parts of electric modulus for HDPE and HDPE+ 10%α-Al_2O_3 are close to each other, 0.33 and 0.34 respectively. The nature of curve remains the same for HDPE+ 10%α-Al_2O_3 but peak shifts to high frequency (10^5Hz) after irradiation which can be attributed to the release of more trapped charge carriers[9]. The M′of other samples show a plateau in intermediate frequency ($5*10^2$ -$2*10^5$Hz) range and gets maximum value at 10^5Hz then decrease to the end of the frequency range.

The frequency dependence of the imaginary parts of electric modulus M″ in alternating fields for pure HDPE and HDPE+ x% α-Al_2O_3 composite containing different amount of filler at D=0 kGy are given in Fig1b. It is found that M″ value firstly decrease with increase of frequency within (25-10^3Hz) frequency range, then remain constant intermediate frequency range 10^3 - 10^5Hz for all examined system, for 3% composites the value of M″increases from 0.003 to 0.009 (3times).

At D=50 kGy exposure dose spectra of M″ exbihit electric modulus relaxation peak around 10^4Hz which is attributed to PE local chain motion [10]. It can be seen from fig1d, the value of M″ decreases at 25-10^3 Hz frequency range, then increase up to 5*10^3 Hz and 10^4Hz, respectively, with the increase frequency value of M″ almost same for all examined system. The relaxation times can be calculated from the relation, $\tau_x = 1/2\pi f_{max}$, for HDPE $\tau_x = 2 \cdot 10^{-4}$s, for 1% $\tau_x = 3 \cdot 10^{-4}$s, for 3,5,10% $\tau_x = 1.6 \cdot 10^{-5}$s. There observed an increase in the value of M″ of composite system. Similar observasions were made for PVDF/$CaCu_3TiO_{12}$ nanocrystal composite[11]. It should be noted that, with increasing irradiation dose up to 50kGy the value of M'' increase 1.4 times measured at 25Hz frequence than 0 kGy, for HDPE M' increases from about 0.007 to 0.005.

From Fig.1f. it can be noted that after 200kGy irradiation peaks shifts to low frequency range in a 0, 1 and 3% composites. There is not peaks 5% and 10% composites. For 0, 1% specimens relaxation time is $\tau_x = 8 \cdot 10^{-4}$s. Also value of M″ increases than 50 kGy irradiation dose in stuied samples. The value of M'' for 10% composites decreases from 0.25 to 0.005 and peak observed at 5*10^6Hz.

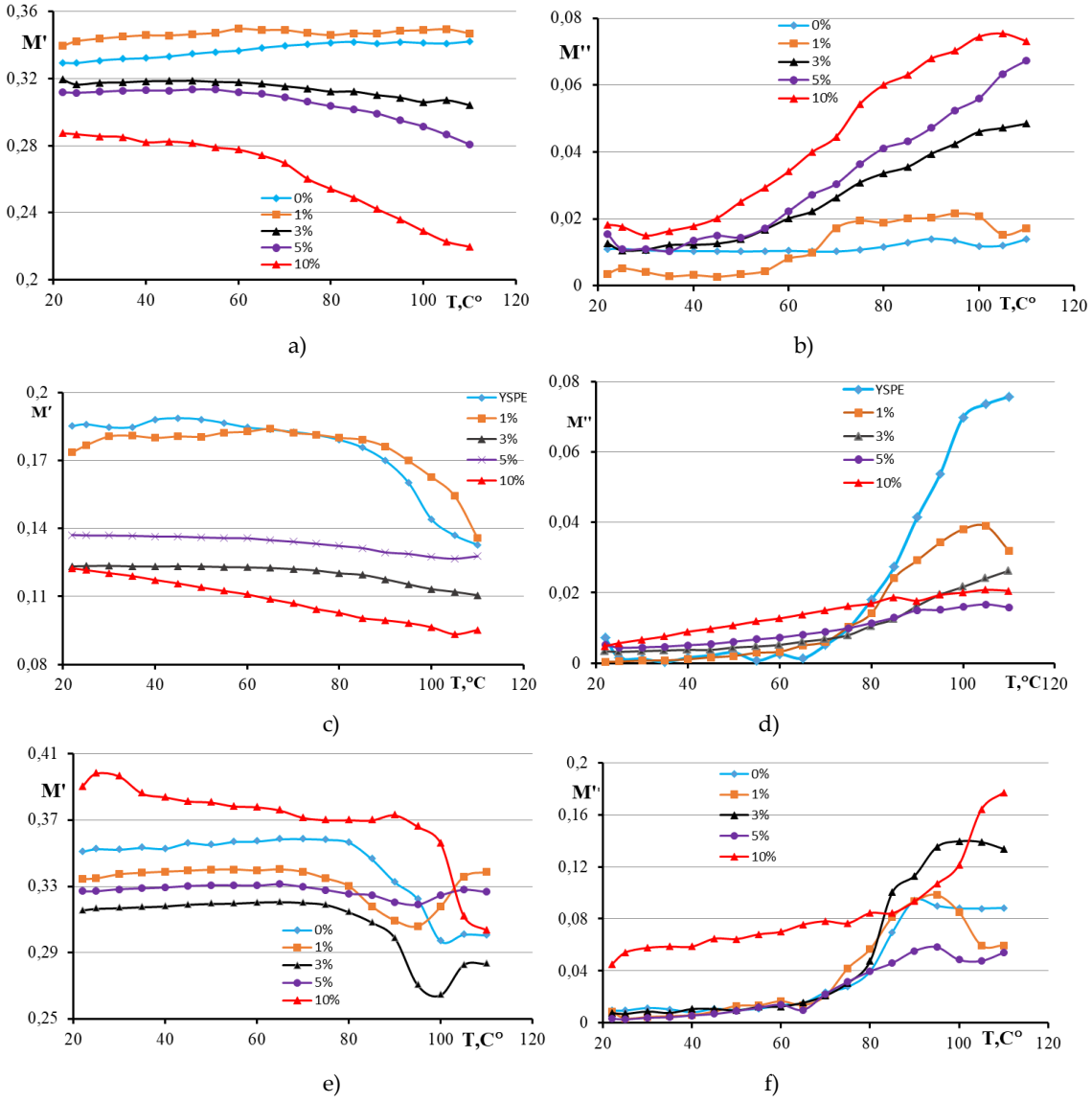

Fig.2. Temperature dependence of real and imaginary parts of electric modulus of HDPE+ x%α-Al_2O_3 at different radiation doses:a,b-0kGy;c,d-50kGy; e,f-200kGy.

Fig. 2 shows the variation of real (M') and imaginary (M'') parts of the electric modulus as a function of temperature for different volume concentrations of α-Al_2O_3 in different doses at costant frequency 10^3Hz . Measurements were made in the temperature range of 20°C-110°C. It can be seen from Figure 1a, the value of M' for pure HDPE and HDPE+1% α-Al_2O_3 composite almost does not change depending on the temperature, the value of M' decreases with increasing temperature at higher temperatures (starting from 60°C), at D=0kGy exposure dose, as the filler content increases in the in the HDPE matrix, at 10% composite the rate of decrease was greater than other samples. The increase of α-Al_2O_3 content results in lower values of M', implying that the real part of dielectric permittivity increases ceramic filler. The value of M'' increases as the filler content increase from 3% to 10% volume percentage in HDPE (Fig.2b.) which is a characteristic of Maxwell-Wagner-Sillar (MWS) relaxation.

In Fig.2c, d M' and M'' as a function of temperature is presented for all the examined systems, after 50kGy γ-irradiation. The value of M' decreases than 0 kGy irradiated samples. It can be seen one relaxation M'' as a function of temperature process, located in the high temperature range are clearly recorded, for pure HDPE, and HDPE +1% α-Al_2O_3 specimens is formed in the temperature range where transition occurs. Thus, values are very close to the glass transition temperature of the pure HDPE. In consequence it is reasonable to suggest the relatively slow dielectric relaxation process corresponds to glass/rubber transition.

Fig.2e, f shows functions M'(T) and M''(T) for HDPE and HDPE+ x% α-Al_2O_3 after γ-irradiation at dose 200kGy. As seen in Fig.2e the value of M' higher than 50kGy irradiated samples. The imaginary part of electric modulus of 0;1 and 3% nanocomposites show plateau in low temperature range (T<80°C), while a broad peak emerges in temperature range of 80°-100°C. Amplitude of peak decreases for 5% composite. Also, value of M'' increases from 0.009 to 0.045 for 10% composite system than pure HDPE and there is not peak in HDPE+ 10% α-Al_2O_3 this temperature range (80°-100°C). It is well known (Aliev, Kh.S., at al., 2018) that α- relaxation process is associated with glass to rubber transition. If sufficient thermal energy is provided to the polymer, then large parts of amorphous macromolecular chains can relax simultaneously in a cooperative motion. The whole process is characterized by glass transition temperature (T_g), which is considered as the temperature where transition occurs. In polymer matrix composite systems, glass transition is related to the chemical structure of the polymer chains and in many cases to the type of the applied filler. As a rule of thumb, glass transition temperature is taken as the temperature at which the α- relaxation loss peak is recorded in the dielectric spectrum at constant frequency.

Conclusion:

The dielectric properties of nanocomposites "nonpolar HDPE/ α-Al_2O_3" were studied within the frequency range of 25–10^6 Hz. It was shown that the dielectric parameters of composites significantly depend on both the α-Al_2O_3 concentration in the polymer and the frequency of the electric field. The appearance of peaks at higher temperature reveals that there may be the MWS-relaxation peak.

REFERENCES

1. H.S.Aliyev, M.M. Guliyev, R.S**.** Ismailova. Relaxation Phenomena in Polyvinylchloride/Graphite Composites. IFAC PapersOnLine 51-30 (2018) 825–827.

2. Fetouhi, L.; Martinez-Vega, J.; Petitgas, B. Electric conductivity, aging and chemical degradation of polyesterimide resins used in the impregnation of rotating machines. IEEE Trans. Electr. Insul. 25, (2018),294–305

3. Fetouhi, L.; Malec, D.; Manfe, P.; Martinez-Vega, J. Experimental Study on the Evolution of Dielectric Properties of Impregnating Varnishes with Thermal Aging. In Proceedings of the IEEE Conference on Electrical Insulation and Dielectric Phenomena (CEIDP), Cancun, Mexico, (21–24 October 2018); 618–621.

4. Tjong, S.C. Structural and mechanical properties of polymer nanocomposites. Mater. Sci. Eng. R Rep. (2006), 53, 73–197.

5. Qi, C.; Yang, W.; He, F.; Yao, J. The Thermal Properties and Degradability of Chiral Polyester-Imides Based on Several l/d-Amino Acids. Polymers (2020), 12, 2053

6. Xia, Y.; Zhou, C.; Wang, W.; Wen, X.; He, S.; Chen, W. Developing a novel environmental friendly polyester-imide impregnating resin. In Proceedings of the IEEE Electrical Insulation Conference (EIC), Seattle, WA, USA, (7–10 June 2015); 551–554.

7. M. Nayef, B. H. Rabee. Effect of plasma irradiation on the electrical characteristics of the PMMA-PS/Al_2O_3 nanocomposites. Digest Journal of Nanomaterials and Biostructures Vol. 18, No. 2, (April - June 2023), 669 – 680.

8. M. Khutia, G.M. Joshi, J. Dielectric relaxation of PVC/PMMA/NiO blends as a function of DC bias. Mater. Sci. Mater. Electron. 26 (2015) 5475-5488.

9. Raghu S, Archana K, Sharanappa C, Ganesh S, Devendrappa. The physical and chemical properties of gamma ray irradiated polymer electrolyte films. Journal of Non-Crystalline Solids,Volume 426, (15 October 2015), 55-62F.

10. Ram Jeewan Sengwa, Shobhna Choudhary. Dielectric and electrical properties of PEO/Al_2O_3 nanocomposites. ournal of Alloys and Compounds 701 (2017) 652-659

11. P. Thomasa,b, K.T. Varughesea, K. Dwarakanatha, K.B.R. Varmab. Dielectric properties of Poly (vinylidene fluoride)/CaCu3Ti4O12composites, Composites Science and Technology 70 (2010) 539–54

JOURNAL OF BAKU ENGINEERING UNIVERSITY - PHYSICS

2024. Volume 8, Number 1 ***Pages 43-49***

UDC: 541.64:539.26:537.529
PACS: 541.183.539.26
DOİ: https://doi.org/10.30546/09081.2024.101.5013

THE EFFECT OF Γ-RADIATION ON THE DIELECTRIC PROPERTIES OF HDPE/ α -SiO_2 COMPOSITES

R.S. ISMAYILOVA, M.M. GULIYEV, A.N. NABIYEVA, N.Sh. ALIYEV, N.N.MEHDIYEVA

Institute of Radiation Problems, Azerbaijan National Academy of Sciences
Az1143, Baku, 9 B. Vahabzade

Karabakh University

Khankendi, Azerbaijan
ismayilovarafiqa5@gmail.com

nargiz.mehdiyeva@karabakh.edu.az

ARTICLE INFO

Article history:
Received: 2024-10-09
Received in revised form: 2024-10-16
Accepted: 2024-11-14
Available online

Keywords:
nanocomposite,
dielectric permittivity,
electrical conductivity,
frequency.

ABSTRACT

The impact of γ-irradiation on the electrical and thermoelectret properties of HDPE/α-SiO_2 nanocomposites was thoroughly studied, with a particular focus on the influence of varying filler concentrations ranging from 0% to 5% by volume. This research aimed to investigate how both the γ-irradiation and the addition of α-SiO_2 nanoparticles affected the overall electrical behavior of the nanocomposite. Key electrical properties such as the dielectric constant (ε'), dielectric loss coefficient (ε"), and alternating current (AC) electrical conductivity (σ) were measured over a broad frequency range spanning from 25 Hz to 1 MHz. Furthermore, the samples were exposed to absorbed γ-radiation doses ranging from 0 to 200 kGy, to evaluate the dose-dependent effects. The results showed that increasing the filler concentration and irradiation dose significantly altered the dielectric and conductive properties, providing valuable insights into the optimization of nanocomposites for various electrical applications. These findings suggest that the controlled use of fillers and irradiation can be used to fine-tune the electrical performance of polymer-based nanocomposites.

ВЛИЯНИЕ Γ-ИЗЛУЧЕНИЯ НА ДИЭЛЕКТРИЧЕСКИЕ СВОЙСТВА КОМПОЗИТОВ HDPE/ α -SiO_2

РЕЗЮМЕ

Влияние γ-облучения на электрические и термоэлектретные свойства нанокомпозитов HDPE/α-SiO_2 было тщательно изучено, с особым акцентом на влияние изменения концентрации наполнителя в диапазоне от 0% до 5% по объему. Целью исследования было выяснить, как γ-облучение и добавление наночастиц α-SiO_2 влияют на общие электрические характеристики нанокомпозита. Основные электрические свойства, такие как диэлектрическая проницаемость (ε′), коэффициент диэлектрических потерь (ε″) и электропроводность переменного тока (σ), измерялись в широком диапазоне частот от 25 Гц до 1 МГц. Кроме того, образцы подвергались воздействию γ-облучения в дозах от 0 до 200 кГр для оценки дозозависимых эффектов. Результаты показали, что увеличение концентрации наполнителя и дозы облучения значительно изменяет диэлектрические и проводящие свойства, предоставляя ценные данные для оптимизации нанокомпозитов для различных электрических применений. Эти выводы предполагают, что контролируемое использование наполнителей и облучения может быть использовано для тонкой настройки электрической производительности полимерных нанокомпозитов.

Ключевые слова: нанокомпозит, диэлектрическая проницаемость, электропроводность, частота.

γ-RADİASİYANIN YSPE/ α-SiO_2 KOMPOZİTLƏRİN DİELEKTRİK XASSƏLƏRİNƏ TƏSİRİ

XÜLASƏ

Yüksək sıxlıqlı polietilen (YSPE) və onun əsasında alınan nanokompozit (YSPE/ α-SiO_2) nümunələrinə γ-şüalanmanın və termoelektret halının təsiri tədqiq edilmişdir. 0-5% həcmində doldurucunun konsentrasiyasının, udulma dozasının və termoelektret halının elektrofiziki xassələrə təsiri müəyyən edilmişdir.Dielektrik nüfuzluğu (ε′), dielektrik itki faktoru (ε″),elektrik keçiriciliyi (σ) $25 \div 10^6$Hs tezlik və 0-200kGr udulma dozası diapozonunda tədqiq edilmişdir. Nəticələr göstərmişdir ki, dolğu konsentrasiyasının və şüalanma dozalarının artması dielektrik və keçirici xassələri əhəmiyyətli dərəcədə dəyişir və bu, nanokompozitlərin müxtəlif elektrik tətbiqləri üçün optimallaşdırılmasına dair mühüm məlumatlar verir. Bu nəticələr göstərir ki, doldurucuların və şüalanmanın nəzarətli istifadəsi polimer əsaslı nanokompozitlərin elektrik performansını incə tənzimləmək üçün istifadə oluna bilər.

Açar sözlər: nanokompozit, dielektrik nüfuzluğu, elektrik keçiriciliyi, tezlik.

Introduction

In recent years, one of the most promising and rapidly developing directions in science and technology has been the production of new nanocomposites. High-density polyethylene (HDPE) and composites based on it are considered indispensable materials in fields such as the atomic and electrical engineering industries, cryogenic technology, medicine, and more. Through various complex methods, nanoparticles are incorporated into the polymer matrix. Such composites exhibit several unique and promising properties (electrophysical, electret, optical). Due to these properties, they are valuable in the development of new sensors, photovoltaic converters, various detectors, piezoelectric materials, and more. Researchers [1, 2] have determined in their studies that adding inorganic nanoparticles to polymers significantly modifies the physical properties of polymer materials, enhancing their applications.

Current research shows that composites obtained by adding nanoparticles at various concentrations, particularly in the range of 1-10%, into the polymer matrix demonstrate superior physical, chemical, mechanical, and dielectric properties compared to the original polymers [3].

In the current era, the interest in composites obtained by adding nanoparticle-based oxide materials to a polymer matrix continues to grow consistently [4]. The addition of ultrafine non-organic particles, such as silicon dioxide (α-SiO_2), to high-density polyethylene (HDPE) further improves the physical and mechanical properties of the polymer [5].

It should be noted that when obtaining a new polymer composite material, it is necessary to investigate the dielectric permeability (ε), dielectric loss (tgδ), and conductivity in both direct (σdc) and alternating (σac) fields after the addition of fillers.

One of the modification methods for high-density polyethylene and the composites obtained from it (HDPE/α-SiO_2) is their irradiation with various types of radiation. Composites modified by ionizing radiation are even more versatile as composite materials. The essence here is the dispersity of the structure and the formation of interphase layers. Due to these characteristics, the application of nanocomposites in micro- and nanoelectronics attracts considerable interest.

The effect of γ-radiation varies depending on the type of polymer. It is known from the literature [6-10] that γ-radiation affects the structure of polyethylene and alters its physicochemical properties, causing irreversible changes in the molecular structure of the polymer. The mechanism of this modification depends on the radiation conditions; it either increases mechanical strength as a result of the construction process in the polymer molecule or leads to molecular fragmentation during the oxidation process.

The increase in dielectric permeability and conductivity in the alternating electric field of HDPE and its composites (HDPE + α-SiO_2) after γ-irradiation is due to the increased density of free radicals and unsaturated bonds. In irradiated samples, the breaking of the molecular chain and the formation of free radicals lead to an increase in the density of unsaturated bonds.

Conducting the Experiment

In the conducted research, high-density polyethylene (HDPE) with a molecular weight of 95 × 10^3 g/mol, a crystallinity degree of 52%, a melting temperature of 130°C, and a density of 958 g/cm^3, marked as 20806-24, and various volumes (Φ=0.1, 3, 5%) of amorphous silicon dioxide (α-SiO_2) nanofiller (Sky Spring Nanomaterials, Inc. Houston, USA) with a specific surface area of S=160 m^2/g, a density of 2.65 g/cm^3, and particle sizes of 20 nm, were prepared as composites using a thermal pressing method. The powdered high-density polyethylene (HDPE) was weighed on a scale in predetermined concentrations together with the nanofiller, then the polymer matrix and the nanofiller were mechanically mixed in a porcelain container until a completely homogeneous mixture was obtained. The resulting homogeneous mixture was subjected to a pressure of 15 MPa at a temperature of 130°C for 5 minutes using a hydraulic press and then cooled in an ice-water mixture [11]. The obtained samples had a thickness of 120-180 μm and a diameter of 40 mm. Some of the samples were initially converted into a thermoelectret state, while others were irradiated with γ-radiation (D=50, 100, 200 kQr). The electrophysical properties (ε, tgδ, σ) of the samples were investigated before and after the thermoelectret formation and γ-radiation exposure.

To obtain the thermoelectret: HDPE and HDPE+α-SiO_2 samples are heated from room temperature to 100°C and kept at this temperature between electrodes in an electric field for 30 minutes. They are then allowed to cool to room temperature, and after cooling, they are freed from the electric field. The surface charge density is measured using a compensation method [12]. The gamma radiation exposure of polymer and composite samples was performed using the MPX-γ-25 device based on the ^{60}Co isotope. The measurement of the electrophysical properties of HDPE and its composites was carried out at frequencies ranging from 25 to 10^6 Hz using an E7-20 type impedance meter, under a constant heating regime for the samples.

The electrophysical properties of HDPE and its composites were clarified concerning frequency, temperature, and dose dependencies at various temperatures.

Discussion of Results

In Figure 1, the dielectric permittivity (ε′) dependencies of HDPE and HDPE+x%α-SiO_2 composites (Fig. 1a) and thermoelectrets (Fig. 1b) before γ-radiation (D=0) are presented as a function of various frequencies. It can be seen from the figure that the dielectric permittivity **(ε′)** values of the initial HDPE and 1% vol. α-SiO_2 nanocomposites are significantly lower compared to the 3% and 5% vol. nanocomposites at 25 Hz. The dielectric permittivity of HDPE and 1% vol. α-SiO_2 nanocomposites does not depend on frequency, meaning that with the increase in frequency, the value of **ε′** changes slightly (decreases). The 3% and 5% vol. samples obtain high values at 25 Hz (5.34 and 6.38, respectively), and with the increase in frequency, it decreases rapidly up to 10^4 Hz, then weakens and stabilizes at the end (10^6 Hz). As the volume percentage of the filler increases (3%; 5%), the value of ε′ increases; however, in the HDPE+5% α-SiO_2 composite, the value of ε′ decreases approximately 1.97 times with increasing frequency. The parameter $\Delta\varepsilon' = (\varepsilon'_c - \varepsilon'_\infty)$, where ε'_c and ε'_∞ are the low and high-frequency dielectric permittivity, respectively, encompasses the entire range of dispersion and is equal to $\Delta\varepsilon' = 3.66$.

In Figure 1b, it is evident that the character of the **ε = f(ν)** dependency does not change; the values of the dielectric permittivity of the initial and 1% vol. samples do not change with increasing frequency, while the ε′ values of the 3% and 5% vol. nanocomposites decrease as frequency increases. The **ε′** values of the 3% and 5% vol. nanocomposites are 4.1 and 3.81, respectively, at 25 Hz. Only for the 5% vol. nanocomposite does the value of ε′ become smaller than that of HDPE and other nanocomposites after the frequency increases beyond 1 kHz (2.66 and 2.18). In the thermoelectret composites (HDPE +5% α-SiO_2), the total width of dispersion is also equal to **Δε′** = 1.68.

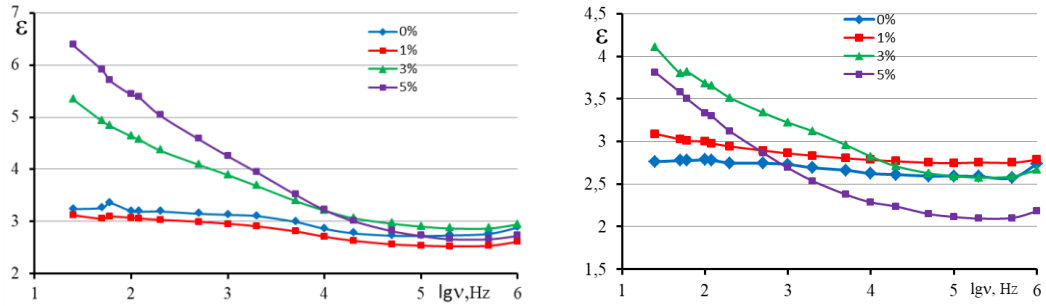

a **b**

Figure 1. The dielectric permittivity (ε) dependence on various frequencies of **HDPE** and **HDPE+α-SiO₂** initial (a) and thermoelectret (b) composites.

If we compare these graphs, we can see that the parameters of the initial composite samples differ from the values obtained for the thermoelectret composites; the dielectric permittivity of HDPE and HDPE +α-SiO_2 nanocomposites is lower for the thermoelectret nanocomposites. At 25 Hz, the value of **ε′** for the 5% vol. samples of thermoelectrets is 3.81, while for the initial composites, it is 6.38.

In Figure 2, the situation of these samples after irradiation with a dose of (D=200 kQr) is shown: it can also be seen that the dielectric permittivity of the initial composites (Φ=5%) is approximately 8 at 25 Hz; meanwhile, the dielectric permittivity of the thermoelectret is approximately 10, which is a noticeable value.

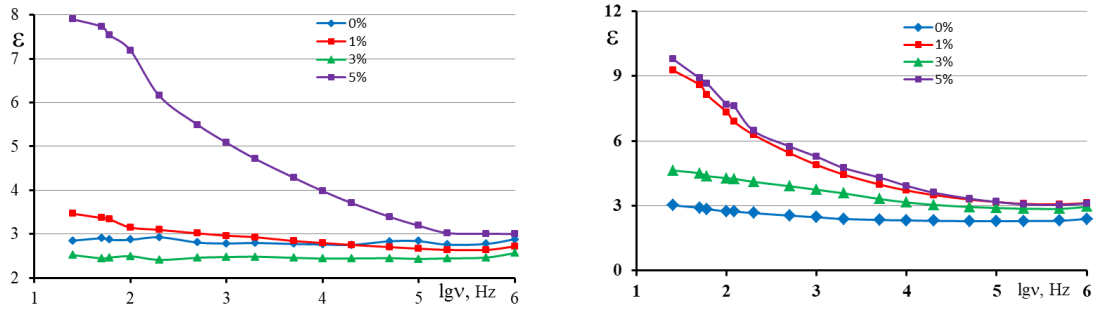

a **b**

Figure 2. The dielectric permittivity **(ε′)** dependence on various frequencies of **HDPE** and **HDPE** +α-SiO_2 ordinary (a) and thermoelectret (b) composites after γ-radiation (D=200 kGr).

From Figures 1-2(a,b), it can be seen that the effect of γ-radiation absorption dose (D=200 kQr) on the dielectric permittivity of HDPE and HDPE +α-SiO_2 composites (Φ=0-5%) is different. As the volume percentage of the filler and the absorption dose increase, the value of ε′ increases. This is most noticeable when the volume percentage of the filler is equal to 5%. Thus, as the volume percentage of the filler increases, the radiation resistance of the composite improves.

After irradiation with D=200 kGr, the following changes are observed in the dependency of $\Delta\varepsilon'=f(\nu)$:

1. In the 1% and 3% samples, the value of ε decreases from 5.34 to 2.52, and no frequency dependence is observed across all frequency ranges.

2. After transitioning to the thermoelectret state and irradiation, the **ε'** values of the 0% and 3% samples increase slightly (from 2.85 to 3.02 for 0%; and from 2.52 to 4.63 for 3%), but no frequency dependence is observed.

3. After irradiation, the value of **ε'** for the 1% and 5% samples increases at low frequencies (from **ε'** = 7.9 to **ε'** = 9.79), then decreases up to 10^5 Hz, followed by stabilization, meaning the stabilization frequency of ε shifts toward higher frequency regions.

Based on the initial analysis of the obtained results, it can be concluded that after irradiation, the increase in ε' and tgδ in HDPE and the composites based on it (HDPE +α-SiO_2) after transitioning to the thermoelectret state can primarily be explained by the increase in the degree of polarization of the samples.

Figures 3-4(a,b) show the dependence of the electrical conductivity of initial and thermoelectret polyethylene and the nanocomposites based on it on the volume percentage of the filler before (Fig. 3, a-b) and after (D=200 kQr) (Fig. 4, a-b) γ-irradiation, expressed as $\boldsymbol{lg\sigma=f(\nu)}$. From the figure (Fig. 3a), it is evident that as the volume percentage of the filler increases, the electrical conductivity (σ) of the composites increases; across all frequency dependencies, the electrical conductivity of the HDPE +α-SiO_2 composites is high. Conversely, after irradiation (D=200 kQr), the electrical conductivity of the thermoelectrets increases (changes); the conductivity of the initial HDPE and HDPE +1%α-SiO_2 composites increases with increasing frequency up to the end of the frequency scale, while in the 3% and 5% volume nanocomposites, this increase continues up to 10^4 Hz and then stabilizes.

In the thermoelectret polymer and nanocomposites (Fig. 3b), the conductivity of the initial (HDPE) and HDPE +1%α-SiO_2 nanocomposites continues to increase significantly, with the conductivity of the 3% and 5% volume nanocomposites being even higher.

After irradiation with a dose of D=200 kGr (Fig.4,a), there are no significant changes in the dependence $\boldsymbol{lg\sigma=f(\nu)}$ for the HDPE sample, while the conductivity values of the 1% and 5% volume samples are higher compared to HDPE and HDPE +3%α-SiO_2 composites.

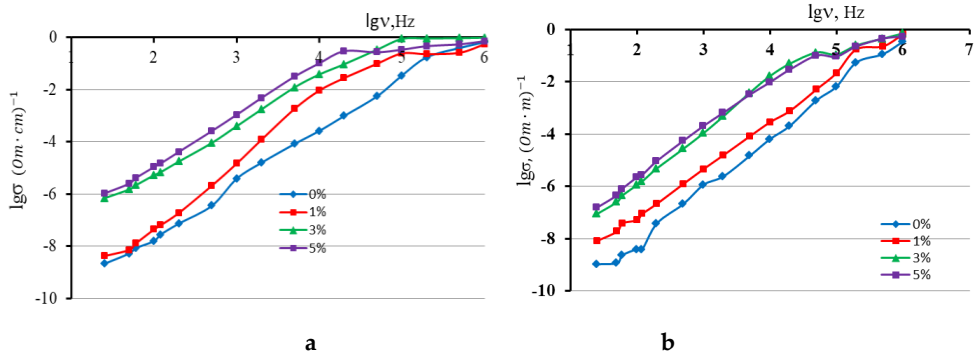

Figure 3. The dependence of electrical conductivity (**σ**) on various frequencies **of HDPE and HDPE +α-SiO_2** initial (a) and thermoelectret (b) composites.

Differences in conductivity are also observed in the thermoelectret polymer and nanocomposites (Fig. 4b), as the conductivity values of HDPE and HDPE +1%α-SiO_2 composites increase from 25 Hz to 10^6 Hz. In contrast, the conductivity of HDPE +5%α-SiO_2 composites begins to increase from 25 Hz, but after 10^4 Hz, the increase weakens. During irradiation, the polymer chains break into smaller segments, during which the crystalline regions are disrupted, and the amorphous regions (phases) begin to increase. At high values of the irradiation dose, the polymer chains break, continually improving the amorphous phase and also generating free radicals, which contributes to the increase in electrical conductivity.

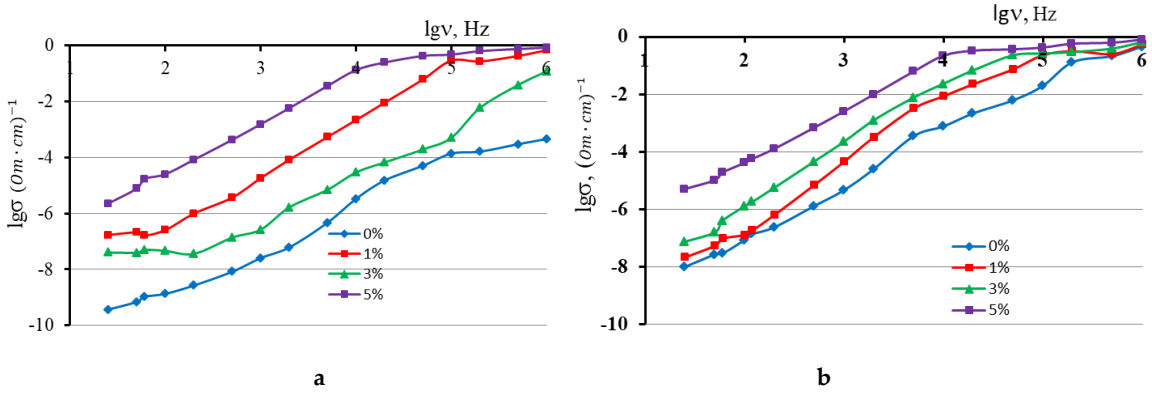

Figure 4. The dependence of electrical conductivity (σ) on various frequencies of HDPE and HDPE +α-SiO_2 ordinary (a) and thermoelectret (b) composites after γ-radiation (D=200 kGr).

In Figures 5 (a,b), the dependence of electrical conductivity on the irradiation dose, $lg\sigma=f(D$ is shown for HDPE, HDPE +α-SiO_2 initial nanocomposites, and HDPE, HDPE +α-SiO_2 composites that have been transformed into thermoelectrets. From the graph, it can be seen (Fig. 5a) that the electrical conductivity of HDPE and HDPE +1%α-SiO_2 nanocomposites changes little with respect to the dose; however, in the 3% α-SiO_2 nanocomposites, while conductivity decreases at a dose of 100 kQr, it increases relatively at a dose of D=200 kQr. The conductivity value in the 5% α-SiO_2 nanocomposite is higher compared to the other composites.

In the thermoelectrets (Fig. 5b), the conductivity values are even higher, especially as both the irradiation dose and the volume percentage of the filler increase, leading to an increase in σ.

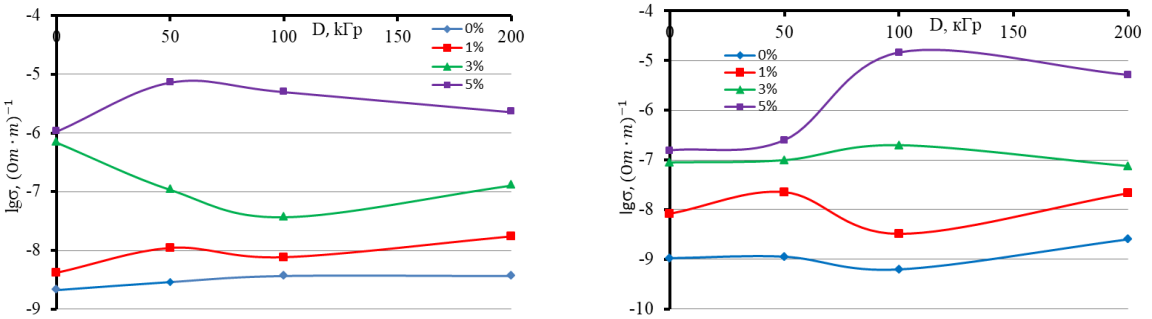

Figure 5. The dependence of electrical conductivity on the dose (D=0-200 kGr) for **HDPE and HDPE +α-SiO_2** initial (a) and thermoelectret (b) composites.

In thermoelectret nanocomposites, the increase in crystalline regions leads to improved mechanical properties and enhanced chemical resistance. Certain changes occur in polyethylene and composites after γ-radiation. As the irradiation dose increases, defects, unsaturated bonds,

and free radicals generated from the degradation of the polymer chain increase, which contributes to the rise in dielectric permittivity. It has also been established that as the irradiation dose increases, the delocalization of carbonyl groups and charge carriers increases, leading to an increase in dielectric permittivity (ε). However, the dielectric permittivity of thermoelectret nanocomposite samples increases significantly.

CONCLUSION:

The effect of γ-irradiation on the electrophysical properties of YSPE+α-SiO2 nanocomposites with various concentrations has been studied. Based on the initial analysis of the obtained results, it can be concluded that after irradiation, YSPE and the composites derived from it (YSPE+α-SiO2) transition to a thermoelectret state, which is characterized by an increase in ε and tgδ. This increase can primarily be attributed to the enhancement of the polarization degree of the samples and the growth of electrical conductivity. After irradiation, a slight increase in the ε value for the 1% and 5% samples at low frequencies is observed, followed by a shift in the stabilization frequency of ε toward higher frequency regions.

REFERENCES

1. S.C.Tjong. Structural and mechanical properties of polymer nanocomposites. Materials Science and Engineering. R. 53(2006) 73-197
2. M.K.Grawford, R.J.Smalley, G.Cohen, B.Hogan, B.Wood, S.K.Kumar, Y.B.Melnichenko, L.He, B.Hammouda. Chain Conformation of polymer nanocomposites with uniformly Dispersed Nanoparticles. Physical Review Letter, PRL, 110, 196001 (2013)
3. H.M.Ahmed, S.H.Ali. Dielectric properties and thermal Conductivity of HDPE and PS. Iraqi, Journal of Science, 2012, v.53, 2, pp 330-334
4. Hussain F., Hojati M., Okamoto M., Gorga R.E. Review article: Polymer –matrix nanocomposites, processing, manufacturing, and application: J Comp Mat. (2006), 40, 1511–1575.
5. R. S. Ismailova, A.M. Magerramov, M. M. Kuliev and G. A. Akhundova. Electrical Conductivity and Dielectric Permittivity of γ-Irradiated Nanocomposites Based on Ultrahigh-Molecular-Weight Polyethylene Filled with α-SiO_2. ISSN 1068-3755, Surface Engineering and Applied Electrochemistry, **54**(2018) , No. 1, pp. 6–11
6. S. Raghu, K.Archana, C.Sharanappa, S.Ganesh, H.Devendrappa. The Physical and Chemical properties of gamma irradiated polymer electrolyte films. J. of Non –Christalline Solids. (2015), 426, pp55-62
7. Toka Swu, Chuba Akum Pongener, Dilpak Sinha, and Noelotpat Sen Sarma. Effect of gamma radiation on dielectric propertiea of poyasetate poymer. Pelagia, Research Library Der Chemica Sinica, (2013), 4(3): 132-136
8. А.П.Тютнев, И.С.Маенко, Е.Д.Пожидаев, Н.С.Костюков. *Диэлектрические свойства полимеров в полях ионизирующих излучений*.М.: Наука, (2005), 188
9. S.Fores. Frequency dependence of the electrical and dielectric constants of polycarbonate (Makrofol-E) film under the effects of γ-radiation. Nat.Center of Radiation Research and Technology (NSRR), AEA, Nasr City, Egypt, **3**(2011) , No12, 1034-1039
10. A.S.Saidov. Thermoelectrically properties the technical Silicon Received by Eightfold Melting on the Solar Furnace.IS Journal Alternative Energy and Ecology, (2010) No3, 83
11. А.М.Магеррамов. Структурное и радиационное модифицирование электретных, пъезоэлектрических свойств полимерных композитов. Баку, Эль, 2001, 327
12. А.Д.Кондратюк. Электретные свойства диэлектриков. Ярославский педагогический вестник, 1998, №3 (15), 109-112

JOURNAL OF BAKU ENGINEERING UNIVERSITY - PHYSICS

2024. Volume 8, Number 1 ***Pages 50-54***

UOT:537.86
PACS: 72.80.Tm
DOI: https://doi.org/10.30546/09081.2024.101.5023

CAPACITANCE-VOLTAGE CHARACTERISTICS OF THE PDSI-SI CONTACT

Afsana E. MAMMADOVA

Baku Engineering University

efsanememmed92@gmail.com

ARTICLE INFO

Article history:
Received: 2024-05-24
Received in revised form: 2024-10-15
Accepted: 2024-10-25
Available online

Keywords: palladium, silicides, Schottky barrier, diode, volt-farad, palladium silicide

ABSTRACT

In the work the volt-amper and volt-farad characteristics of PdSi-Si contact have been studied. The possibility for definition of series of important parameters for Pd, Si and PdSi by means of these characteristics has been considered. The linearity of the experimental dependence of $1/C^2$ on a voltage and equability of distribution for impurities in the near surface area of a semiconductor have been established.

The value of the acceptor concentration determined from the slope of the current-voltage characteristic coincides with the value calculated from the resistivity of silicon

Conducted studies of the dependence of capacitance on voltage showed that in the range of 300 -106 Hz the capacitance practically does not depend on frequency

During the measurement process, R < R was carried out, that is, the measurement limit of the electrometric amplifier was selected

ВОЛЬТ-ЕМКОСТНЫЕ ХАРАКТЕРИСТИКИ КОНТАКТА PDSI-SI

РЕЗЮМЕ

В работе исследованы вольт-фарадные характеристики контакта PdSi-Si. Рассмотрена возможность определения ряда важных параметров для Pd, Si и PdSi с помощью этих характеристик. Установлены линейность экспериментальной зависимости $1/C^2$ от напряжения и равномерность распределения примесей в приповерхностной области полупроводника

Значение концентрации акцепторов, определенное по наклону вольт-амперной характеристики, совпадает со значением, рассчитанным по удельному сопротивлению кремния.

Проведенные исследования зависимости емкости от напряжения показали, что в диапазоне 300-106 Гц емкость практически не зависит от частоты.

В процессе измерения осуществлялось R < R, то есть выбирался предел измерения электрометрического усилителя.

Ключевые слова: палладий, силициды, барьер Шоттки, диод, вольт-фарад, силицид палладия.

PDSİ-Sİ KONTAKTIN VOLT-FARAD XARAKTERİSTİKALARI

XÜLASƏ

İşdə PdSi-Si kontaktın volt-farad xarakteristikaları öyrənilmiş, həmin xarakteristikaların köməyi ilə Pd, Si və PdSi üçün bir sıra vacib fiziki parametrlərin təyin edilməsi imkanlarına baxılmışdır. $1/C^2$ – nın gərginlikdən eksperimental asılılığının xətti xarakter daşıması və yarımkeçiricinin səthə yaxın oblastında ionlaşmış aşqarların bərabər paylanması müəyyən edilmişdir.

Cari gərginlik xarakteristikasının oblastında müəyyən edilən qəbuledici konsentrasiyanın dəyəri silisiumun müqavimətindən hesablanan dəyərlə üst-üstə düşür.

Kapasitansın gərginlikdən asılılığına dair aparılan tədqiqatlar göstərdi ki, 300-106 Hz diapazonunda tutum praktiki olaraq tezlikdən asılı deyil.Ölçmə prosesi zamanı R < R həyata keçirildi, yəni elektrometrik gücləndiricinin ölçmə həddi seçildi.

Açar sözlər: *palladium, silisidlər, Şotki barieri, diod, volt-farad, palladium silisid*

Introduction

More information about the mechanism of charge transfer is provided by studying the temperature dependence of the current-voltage characteristics. To measure the temperature dependences, the samples were placed in a thermostat, the power of which was supplied from an autotransformer. The sample temperature was controlled by a chromel aluminum thermocouple mounted directly on the plate. Before taking the temperature characteristics, the effect of heat treatment on the electrical properties of the devices was studied. It turned out that heat treatment of the structure up to 200 C does not cause irreversible changes in the electrical properties of PdSi

In order to prevent premature breakdown caused by an increase in the electric field at the periphery of the contact, diffusion guard rings with a depth of 0.5 μm were used. Although the breakdown voltage was increased from 12 to 30 V, there was no saturation when the palladium-silicon silicide barber reversed current.

Physicochemical processes occurring at the palladium silicide-silicon interface greatly affect the uniformity of the contact. When PdSi is formed, the volume decreases by 13% compared to the volume of palladium and silicon reacting. Such differences in crystal chemical properties can create favorable conditions for the introduction of both palladium atoms and impurity atoms in the surface layer of silicon. We assume that the introduction of impurity atoms into the surface layer of silicon leads to inhomogeneity at the PdSi-Si interface.

The Schottky barrier height of PdSi-Si ideal diodes lies in the range of 0.70-0.79 eV. At the same time, the results of our measurements showed that the barrier height for PdSi-Si obtained by magnetron sputtering is 0.79 eV. It is for this reason that the breakdown voltage does not depend on the thickness of the palladium silicide obtained by magnetron sputtering, which indicates the homogeneity of the PdSi-Si contact.

The work investigated the electrical properties of PdSi-Si structures obtained both by thermal evaporation and by magnetron evaporation. The current flowing through the Schottky diode was measured by the voltage drop across the output resistance of the electrometric amplifier connected in series with the diode under study and the power source. The amplifier's input impedances were pre-calibrated by comparing their nominal values with the reference impedances.The main difficulty in measuring high-resistance samples is the inability to directly measure the voltage on the sample, since connecting a voltmeter with a low input resistance to the sample leads to a significant current leakage through the voltmeter.In this work, a TR-1657 digital voltmeter was used for measurements, which has an input resistance less than the resistance of the sample being measured. The voltmeter was connected in parallel to a chain consisting of two series-connected resistances of the amplifier input resistance R_g and the sample resistance R_n.

During the measurement process, R < R was carried out, that is, the measurement limit of the electrometric amplifier was selected at which its input resistance turned out to be significantly less than the resistance turned out to be significantly less than the resistance of the sample and the voltmeter essentially recorded the voltage on the sample.

Figure 1 shows the current-voltage characteristic of the PdSi-Si contact obtained by thermal evaporation.

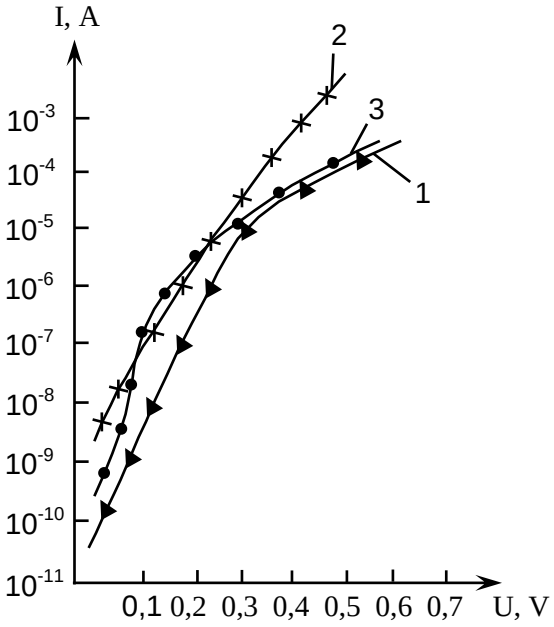

Fiq.VAX struktur 300^{0}C, 2-350^{0}C, 3-400^{0}C

Measurements of capacitance-voltage characteristics (CVC) are among the most common methods for studying semiconductor devices [1]. Using these characteristics, a number of important physical parameters inherent in both structures and the materials from which they are made are determined. Of particular interest is the study of CV characteristics filmed in dynamic mode. The main advantage of this method is the possibility of direct measurement of C(U), ∂C(U)/∂U and other characteristics, which can significantly increase accuracy.

The device is assembled according to the block diagram proposed in [2]. The structure under study (Fig. 2) is included in a bridge circuit to which a sinusoidal test signal UT =U0Sinωt with amplitude UT ≤ kT/q and sawtooth voltage U = αt + const is supplied.

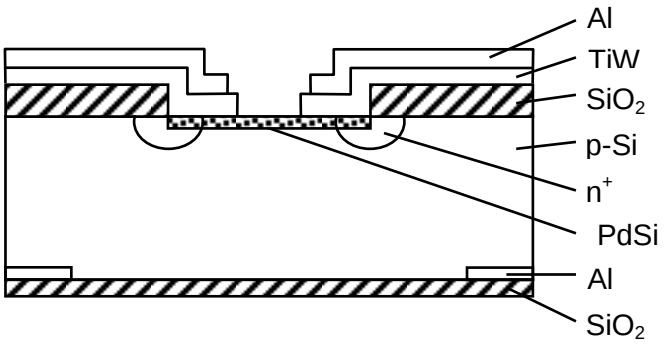

Fig.2 Cross section of a PdSi-p-Si based Schottky diode

The load resistance value was selected from the condition RH > > (ωck)-1 for the test signal and the reverse for the sawtooth voltage. The signal taken from the load RH1, equal to UH = const (Y + jωC), after preliminary amplification, is fed to the detector to isolate the impedance components. The signal from the second arm of the measuring circuit, consisting of the reference capacitance SET and load resistance KN2, is supplied to the input of amplifier U2, amplified and rectified by the detector. The detected signals are fed to the inputs of the comparator and compared. The output of the comparator is connected through differentiating RC chains to the

input of the oscilloscope. In this case, the output voltage of the comparator remains constant as long as SET ≠ Cx, and the signal at the oscilloscope input is equal to 0. At some voltage offset, the reference capacitance SET = Cx(U) and a signal appears at the output of the comparator that unlocks the grids of the cathode ray tube of the oscilloscope.

Figure 3 shows an oscillogram of the capacitance-voltage characteristics of PdSi-p-Si structures at a frequency of 1 MHz.

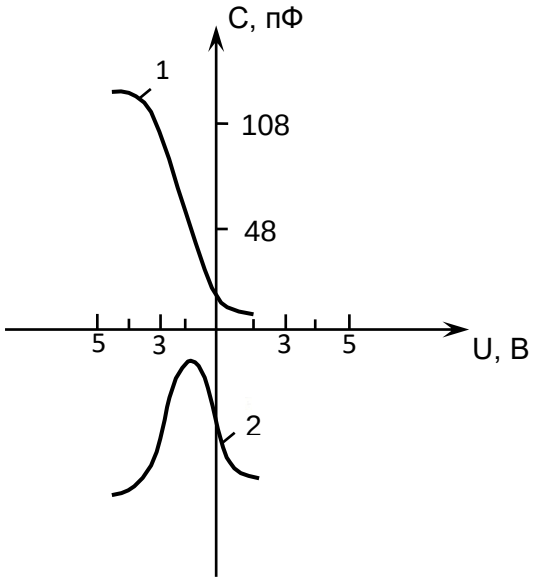

Fig. 3 Current-voltage characteristics of PdSi–n–Si structures

Conducted studies of the dependence of capacitance on voltage showed that in the range of 300 -106 Hz the capacitance practically does not depend on frequency and varies according to the law:

$$C = (q\varepsilon_n N_A / 2)^{1/2} (V_{d0} + V_{obr} - kT / q)^{1/2}$$

The position of the Fermi level ξ, as well as the barrier height, can be calculated from the value of NA obtained from the slope of the dependence of S/c2 on U.

Because the:

$$\xi = (kT/ q)\ln(N_v/N_A)$$

In the absence of bias voltage, the action of mirror image forces reduces the height of the barrier by:

$$\Delta \varphi_{Bi} = [q^3 \varepsilon_n / 2\pi^2(\varepsilon^{|}_n)^2 (\varphi_B - \varepsilon_f - kT/ q)]^{1/4}$$

And the superposition of the mirror image forces acting on the carriers and the electric field of the depletion layer leads to a shift of the barrier maximum by:

$$x_м = 1/4 [q \varepsilon^{|}_n (\varphi_B - \varepsilon_f - kT/ q)/ 2\pi^2(\varepsilon^{|}_n)^2 N_A]^{1/4}$$

The dependence of the I/C2 ratio on the applied voltage for the same diodes is shown in Fig. 18. As can be seen from the figure, the experimental dependence of I/C2 on is linear, which indicates a uniform distribution of ionized impurities in the near-surface region of the

semiconductor. The value of the acceptor concentration NA=IOI5 cm-3/ determined from the slope of the current-voltage characteristic coincides with the value calculated from the resistivity of silicon /ϱ=IO Ohm*cm corresponds to NA=I.5.IOI5 cm-3/, which indicates the absence of doping and the formation of electrically active defects in the near-surface region of silicon during the formation of silicide

Conclusion: the results of our measurements showed that the barrier height for PdSi-Si obtained by magnetron sputtering is 0.79 eV. It is for this reason that the breakdown voltage does not depend on the thickness of the palladium silicide obtained by magnetron sputtering, which indicates the homogeneity of the PdSi-Si contact. The work investigated the electrical properties of PdSi-Si structures obtained both by thermal evaporation and by magnetron evaporation

REFERENCES

1. S.P. Wakefield, U.S.Patents #6, 417, 657, 20 April 2021
2. L.P. Testardi, J. Appl.Phys,51, 5770, (2020)
3. J.M. Poate, J.C.Bean, Jpn J. Appl.Phys, 23,821(2022)
4. E.V. Lam and A.F.Tasch, Jr.J.Electrochem.Soc.217, 2020.
5. E.Ə. Kərimov., Ş.Ə.Bayramova. PtSi kontaktı əsasında Şottki fotodiodlarının effektivliyinin artırılmasının fiziki əsasları. -Azerbaijan Journal of Physics Fizika, Volume XVI, Number 3-4, Series: Az, December,2010, pp.15-16.
6. Mekhtiev T.E., Kasymov N.F. Photodetektor on PtSi-Si Basis with Coding Device. – Turkish Journal of Physics, v.20, №8, 1996, pp.891-895.
7. Kazımov N.F., İskəndərov A.İ., Ələkbərova S.Y., Məlikov T.H., Paşayev N.M., Sadıqova İ.S., Xidirov A.Ş. PtSi-SiO_2 əsasında fotoelementin alınması texnologiyası. MAKA – nın Xəbərləri Tom 8, № 2 (8), Bakı-2005,s.165 – 168.
8. Международной научно – технической конференции, Микроэлектронные преобразователи и приборы на их основе, 27-29 ноября 2013 г. Баку – Сумгаит.
9. Т.Э.Мехтиев, Н.Ф.Казымов, Р.Г.Джафарова, М.Ф.Казымова. Получение контактов с барьером Шоттки на основе силицида платины-кремний. Сообщения НПО Космических исследований. Баку, 1987, ст.116
10. Н.Ф.Казимов.,А.Ф.Мамедова.,С.Э.Джалалова.,Д.И.Алиева. Электрические свойства наноконтакта с барьером Шоттки на основе силицида иридия-кремний. Известия Азербайджжанского Национального Аэрокосмического Агентства. Т18, 2015, № 2(18) ст.80-82.
11. Полевщикова Н.И, Тенденции развития фокальных ИК- матриц на основе силицидов металлов с барьером Шоттки. Выпуск 101, Фактолграфическая справка №117/85, ОНТИ предприятия условных индекс 216, 2014.
12. M.Menon, D.S. Srivastava. Carbon nanotube based molecular electronic devices. J. Mater. Res., 13, 9, 2357-2361 (2001).
13. Полевщикова Н.И, Тенденции развития фокальных ИК- матриц на основе силицидов металлов с барьером Шоттки. Выпуск 101, Фактолграфическая справка №117/85, ОНТИ предприятия условных индекс 216, 2014.
14. SaitoRet.al. Appl. Phys. Lett. 60 2204 (1992).3, 2013, s. 395.
15. Chau R., Boyanov B., Doyle B. Silicon nano-transistors for logic applications // Physica E: Low-dimensional Systems and Nanostructures. 2003.V.19.№.1-2. p.1-5.
16. Aliyeva R.A., Pashaev F.G., Gasanovv A.G., Makmudov K.T. Quantum – Chemical Calculation of the Tautomeric Forms of B Derivatives of Acetylacetone and Determination of the Stability Constants of their Complexes with R%are – Eart Metals // Russian J.of Coordination Chem ., 2009, v.35, p.241-246.

INSTRUCTIONS FOR AUTHORS

1. "The Baku Engineering University Journal-Physics" accepts original unpublished articles and reviews in the research field of the author.
2. Articles are accepted in English.
3. File format should be compatible with **Microsoft Word** and must be sent to the electronic mail (**journal@beu.edu.az**) of the Journal. The submitted article should follow the following format:

- Article title, author's name and surname
- The name of workplace
- Mail address
- Abstract and key words

4. The title of the article should be in each of the three languages of the abstract and should be centred on the page and in bold capitals before each summary.
5. **The abstract** should be written in **9 point** type size, between **100** and **150** words. The abstract should be written in the language of the text and in two more languages given above. The abstracts of the article written in each of the three languages should correspond to one another. The keywords should be written in two more languages besides the language of the article and should be at least three words.
6. . **UDC** and **PACS** index should be used in the article.
7. The article must consist of the followings:

- Introduction
- Research method and research
- Discussion of research method and its results
- In case the reference is in Russian it must be given in the Latin alphabet with the original language shown in brackets.

8. **Figures, pictures, graphics and tables** must be of publishing quality and inside the text. Figures, pictures and graphics should be captioned underneath, tables should be captioned above.
9. **References** should be given in square brackets in the text and listed according to the order inside the text at the end of the article. In order to cite the same reference twice or more, the appropriate pages should be given while keeping the numerical order. For example: [7, p.15].

Information about each of the given references should be full, clear and accurate. The bibliographic description of the reference should be cited according to its type (monograph, textbook, scientific research paper and etc.) While citing to scientific research articles, materials of symposiums, conferences and other popular scientific events, the name of the article, lecture or paper should be given.

Samples:

a) ***Article:*** Demukhamedova S.D., Aliyeva İ.N., Godjayev N.M.. *Spatial and electronic structure af monomerrik and dimeric conapeetes of carnosine üith zinc,* Journal of structural Chemistry, Vol.51, No.5, p.824-832, 2010

b) ***Book:*** Christie ohn Geankoplis. *Transport Processes and Separation Process Principles*. Fourth Edition, Prentice Hall, p.386-398, 2002

c) ***Conference paper:*** Sadychov F.S., Aydın C., Ahmedov A.İ.. Appligation of Information – Commu-nication Technologies in Science and education. II International Conference."*Higher Twist Effects In Photon- Proton Collisions", Bakı, 01-03 Noyabr, 2007, ss 384-391*

References should be in 9-point type size.

10. The margins sizes of the page: - Top 2.8 cm. bottom 2.8 cm. left 2.5 cm, right 2.5 cm. The article main text should be written in Palatino Linotype 11 point type size single-spaced. Paragraph spacing should be 6 point.
11. The maximum number of pages for an article should not exceed 15 pages
12. The decision to publish a given article is made through the following procedures:

- The article is sent to at least to experts.
- The article is sent back to the author to make amendments upon the recommendations of referees.
- After author makes amendments upon the recommendations of referees the article can be sent for the publication by the Editorial Board of the journal.

YAZI VƏ NƏŞR QAYDALARI

1. "Journal of Baku Engineering University" Fizika- əvvəllər nəşr olunmamış orijinal əsərləri və müəllifin tədqiqat sahəsi üzrə yazılmış icmal məqalələri qəbul edir.
2. Məqalələr İngilis dilində qəbul edilir.
3. Yazılar **Microsoft Word** yazı proqramında, (**journal@beu.edu.az**) ünvanına göndərilməlidir. Göndərilən məqalələrdə aşağıdakılara nəzərə alınmalıdır:

- Məqalənin başlığı, müəllifin adı, soyadı,
- İş yeri,
- Elektron ünvanı,
- Xülasə və açar sözlər.

4. **Məqalədə başlıq hər xülasədən əvvəl** ortada, qara və böyük hərflə xülasələrin yazıldığı hər üç dildə olmalıdır.
5. **Xülasə** 100-150 söz aralığında olmaqla, 9 punto yazı tipi böyüklüyündə, məqalənin yazıldığı dildə və bundan əlavə yuxarıda göstərilən iki dildə olmalıdır. Məqalənin hər üç dildə yazılmış xülasəsi bir-birinin eyni olmalıdır. Açar sözlər uyğun xülasələrin sonunda onun yazıldığı dildə verilməklə ən azı üç sözdən ibarət olmalıdır.
6. Məqalədə UOT və PACS kodları göstərilməlidir.
7. Məqalə aşağıdakılardan ibarət olmalıdır:

- Giriş,
- Tədqiqat metodu
- Tədqiqat işinin müzakirəsi və onun nəticələri,
- İstinad ədəbiyyatı rus dilində olduğu halda orjinal dili mötərzə içərisində göstərməklə yalnız Latın əlifbası ilə verilməlidir.

8. **Şəkil**, **rəsm**, **grafik** və **cədvəllər** çapda düzgün, aydın çıxacaq vəziyyətdə və mətn içərisində olmalıdır. Şəkil, rəsm və grafiklərin yazıları onların altında yazılmalıdır. Cədvəllərdə başlıq cədvəlin üstündə yazılmalıdır.
9. **Mənbələr** mətn içərisində kvadrat mötərizə daxilində göstərilməklə məqalənin sonunda mətn daxilindəki sıra ilə düzülməlidir. Eyni mənbəyə iki və daha cox istinad edildikdə əvvəlki sıra sayı saxlanmaqla müvafiq səhifələr göstərilməlidir. Məsələn: [7,səh.15].

Ədəbiyyat siyahısında verilən hər bir istinad haqqında məlumat tam və dəqiq olmalıdır. İstinad olunan mənbənin biblioqrafik təsviri onun növündən (monoqrafiya, dərslik, elmi məqalə və s.) asılı olaraq verilməlidir. Elmi məqalələrə, simpozium, konfrans, və digər nüfuzlu elmi tədbirlərin materiallarına və ya tezislərinə istinad edərkən məqalənin, məruzənin və ya tezisin adı göstərilməlidir.

Nümunələr:

a) ***Məqalə:*** Demukhamedova S.D., Aliyeva İ.N., Godjayev N.M.. *Spatial and electronic structure af monomeric and dimeric complexes of carnosine with zinc,* Journal of structural Chemistry, Vol.51, No.5, p.824-832, 2010

b) ***Kitab:*** Christie ohn Geankoplis. *Transport Processes and Separation Process Principles*. Fourth Edition, Prentice Hall, 2002

c) ***Konfrans:*** Sadychov F.S., Aydın C., Ahmedov A.İ.. Appligation of Information-Communication Technologies in Science and education. II International Conference. "*Higher Twist Effects In Photon- Proton Collisions", Bakı, 01-03 Noyabr, 2007, ss 384-391*

Mənbələr 9 punto yazı tipi böyüklüyündə olmalıdır.

10. **Səhifə ölçüləri:** üstdən 2.8 sm, altdan 2.8 sm, soldan 2.5 sm və sağdan 2.5 sm olmalıdır. Mətn 11 punto yazı tipi böyüklüyündə, **Palatino Linotype** yazı tipi ilə və tək simvol aralığında yazılmalıdır. Paraqraflar arasında 6 punto yazı tipi aralığında məsafə olmalıdır.
11. Orijinal tədqiqat əsərlərinin tam mətni bir qayda olaraq 15 səhifədən artıq olmamalıdır.
12. Məqalənin nəşrə təqdimi aşağıdakı qaydada aparılır:

- Hər məqallə ən azı iki ekspertə göndərilir.
- Ekspertlərin tövsiyələrini nəzərə almaq üçün məqalə müəllifə göndərilir.
- Məqalə, ekspertlərin tənqidi qeydləri müəllif tərəfindən nəzərə alındıqdan sonra Jurnalın Redaksiya Heyəti tərəfindən çapa təqdim oluna bilər.

YAZIM KURALLARI

1. "Journal of Baku Engineering University-Physics" önceler yayımlanmamış orijinal çalışmaları ve yazarın kendi araştırma alanın-da yazılmış derleme makaleleri kabul etmektedir.
2. Makaleler İngilizce kabul edilir.
3. Makaleler Microsoft Word yazı programında, (**journal@beu.edu.az**) adresine gönderilmelidir. Gönderilen makalelerde şunlar dikkate alınmalıdır:

- Makalenin başlığı, yazarın adı, soyadı,
- İş yeri,
- E-posta adresi,
- Özet ve anahtar kelimeler.

4. **Özet** 100-150 kelime arasında olup 9 font büyüklüğünde, makalenin yazıldığı dilde ve yukarıda belirtilen iki dilde olmalıdır. Makalenin her üç dilde yazılmış özeti birbirinin aynı olmalıdır. Anahtar kelimeler uygun özetin sonunda onun yazıldığı dilde verilmekle en az üç sözcükten oluşmalıdır.
5. Makalede UOT ve PACS tipli kodlar gösterilmelidir.
6. Makale şunlardan oluşmalıdır:

- Giriş,
- Araştırma yöntemi
- Araştırma
- Tartışma ve sonuçlar,
- İstinat Edebiyatı Rusça olduğu halde orjinal dili parantez içerisinde göstermekle yalnız Latin alfabesi ile verilmelidir.

7. **Şekil, Resim, Grafik** ve **Tablolar** baskıda düzgün çıkacak nitelikte ve metin içerisinde olmalıdır. Şekil, Resim ve grafiklerin yazıları onların alt kısımda yer almalıdır. Tablolarda ise başlık, tablonun üst kısmında bulunmalıdır.
8. **Kullanılan kaynaklar**, metin dâhilinde köşeli parantez içerisinde numaralandırılmalı, aynı sırayla metin sonunda gösterilmelidir. Aynı kaynaklara tekrar başvurulduğunda sıra muhafaza edilmelidir. Örneğin: [7,seh.15].

Referans verilen her bir kaynağın künyesi tam ve kesin olmalıdır. Referans gösterilen kaynağın türü de eserin türüne (monografi, derslik, ilmî makale vs.) uygun olarak verilmelidir. İlmi makalelere, sempozyum, ve konferanslara müracaat ederken makalenin, bildirinin veya bildiri özetlerinin adı da gösterilmelidir.

Örnekler:

a) ***Makale:*** Demukhamedova S.D., Aliyeva İ.N., Godjayev N.M.. *Spatial and Electronic Structure of Monomerik and Dimeric Conapeetes of Carnosine Üith Zinc,* Journal of Structural Chemistry, Vol.51, No.5, p.824-832, 2010

b) ***Kitap:*** Christie ohn Geankoplis. *Transport Processes and Separation Process Principles.* Fourth Edition, Prentice Hall, p.386-398, 2002

c) ***Kongre:*** Sadychov F.S., Aydın C., Ahmedov A.İ. Appligation of Information-Communication Technologies in Science and education. II International Conference. "*Higher Twist Effects In Photon- Proton Collisions", Bakı, 01-03 Noyabr, 2007, ss 384-391*

Kaynakların büyüklüğü 9 punto olmalıdır.

9. **Sayfa ölçüleri**; üst: 2.8 cm, alt: 2.8 cm, sol: 2.5 cm, sağ: 2.5 cm şeklinde olmalıdır. Metin 11 punto büyüklükte **Palatino Linotype** fontu ile ve tek aralıkta yazılmalıdır. Paragraflar arasında 6 puntoluk yazı mesafesinde olmalıdır.
10. Orijinal araştırma eserlerinin tam metni 15 sayfadan fazla olmamalıdır.
11. Makaleler dergi editör kurulunun kararı ile yayımlanır. Editörler makaleyi düzeltme için yazara geri gönderilebilir.
12. Makalenin yayına sunuşu aşağıdaki şekilde yapılır:

- Her makale en az iki uzmana gönderilir.
- Uzmanların tavsiyelerini dikkate almak için makale yazara gönderilir.
- Makale, uzmanların eleştirel notları yazar tarafından dikkate alındıktan sonra Derginin Yayın Kurulu tarafından yayına sunulabilir.

13. Azerbaycan dışından gönderilen ve yayımlanacak olan makaleler için,(derginin kendilerine gonderilmesi zamani posta karşılığı) 30 ABD Doları veya karşılığı TL, T.C. Ziraat Bankası/Üsküdar-İstanbul 0403 0050 5917 No'lu hesaba yatırılmalı ve makbuzu üniversitemize fakslanmalıdır.

ПРАВИЛА ДЛЯ АВТОРОВ

1. «Journal of Baku Engineering University» - Физика публикует оригинальные, научные статьи из области исследования автора и ранее не опубликованные.
2. Статьи принимаются на английском языке.
3. Рукописи должны быть набраны согласно программы **Microsoft Word** и отправлены на электронный адрес **(journal@beu.edu.az)**. Отправляемые статьи должны учитывать следующие правила:

- Название статьи, имя и фамилия авторов
- Место работы
- Электронный адрес
- Аннотация и ключевые слова

4. **Заглавие статьи** пишется для каждой аннотации заглавными буквами, жирными буквами и располагается по центру. Заглавие и аннотации должны быть представлены на трех языках.
5. **Аннотация**, написанная на языке представленной статьи, должна содержать 100-150 слов, набранных шрифтом 9 punto. Кроме того, представляются аннотации на двух других выше указанных языках, перевод которых соответствует содержанию оригинала. Ключевые слова должны быть представлены после каждой аннотации на его языке и содержать не менее 3-х слов.
6. В статье должны быть указаны коды UOT и PACS.
7. Представленные статьи должны содержать:

- Введение
- Метод исследования
- Обсуждение результатов исследования и выводов.
- Если ссылаются на работу на русском языке, тогда оригинальный язык указывается в скобках, а ссылка дается только на латинском алфавите.

8. **Рисунки, картинки, графики и таблицы** должны быть четко выполнены и размещены внутри статьи. Подписи к рисункам размещаются под рисунком, картинкой или графиком. Название таблицы пишется над таблицей.
9. **Ссылки** на источники даются в тексте цифрой в квадратных скобках и располагаются в конце статьи в порядке цитирования в тексте. Если на один и тот же источник ссылаются два и более раз, необходимо указать соответствующую страницу, сохраняя порядковый номер цитирования. Например: [7, стр.15]. Библиографическое описание ссылаемой литературы должно быть проведено с учетом типа источника (монография, учебник, научная статья и др.). При ссылке на научную статью, материалы симпозиума, конференции или других значимых научных мероприятий должны быть указаны название статьи, доклада или тезиса.

Например:

a) ***Статья:*** Demukhamedova S.D., Aliyeva I.N., Godjayev N.M. *Spatial and electronic structure of monomeric and dimeric complexes of carnosine with zinc,* Journal of Structural Chemistry, Vol.51, No.5, p.824-832, 2010

b) ***Книга:*** Christie on Geankoplis. *Transport Processes and Separation Process Principles.* Fourth Edition, Prentice Hall, 2002

c) ***Конференция:*** Sadychov F.S, Fydin C,Ahmedov A.I. Appligation of Information-Communication Nechnologies in Science and education. II International Conference. *"Higher Twist Effects In Photon-Proton Collision",* Bakı,01-03 Noyabr, 2007, ss.384-391

Список цитированной литературы набирается шрифтом 9 punto.

10. **Размеры страницы:** сверху 2.8 см, снизу 2.8 см, слева 2.5 и справа 2.5. Текст печатается шрифтом **Palatino Linotype**, размер шрифта 11 punto, интервал-одинарный. Параграфы должны быть разделены расстоянием, соответствующим интервалу 6 punto.
11. Полный объем оригинальной статьи, как правило, не должен превышать 15 страниц.
12. Представление статьи к печати производится в ниже указанном порядке:

- Каждая статья посылается не менее двум экспертам.
- Статья посылается автору для учета замечаний экспертов.
- Статья, после того, как автор учел замечания экспертов, редакционной коллегией журнала может быть рекомендована к печати.